CHAPTER 6

Modeling of Stratospheric Aerosols

Lead Authors:
Debra Weisenstein
Slimane Bekki

Authors:
Michael Mills
Giovanni Pitari
Claudia Timmreck

Contributors:
Mian Chin
Mark Hervig
Fok-Yan Leung
Beiping Luo
Eva Mancini
Joyce Penner
James C. Wilson

6.1 Summary

- Models provide a way to synthesize our knowledge of stratospheric aerosol processes and quantitatively test our understanding against observations. However, model uncertainties, especially transport rates, limit our confidence.
- Sedimentation is a crucial process determining the vertical distribution of aerosol mass and sulfur in the stratosphere. Sedimentation is a strong function of altitude as well as particle size, and reduces sulfur in the upper model stratospheres by over 75%.
- Nucleation of new particles is important near the tropopause, particularly in the tropics, and at polar latitudes in the middle stratosphere in winter. Particle size is determined by nucleation, and subsequently by coagulation, condensation, and evaporation, as well as transport and mixing.
- OCS, SO_2, and particles transported across the tropopause are the primary precursors to stratospheric aerosol. Analysis of sulfur budgets in the models shows that transport of SO_2 and particles, for which SO_2 is the precursor, across the tropical tropopause are potentially large contributors to the stratospheric aerosol burden. Large uncertainties remain in our ability to quantify the relative contributions, but the models show OCS to be the main contributor above 25 km and SO_2 and particles to play a larger role below.
- OCS mixing ratios in the tropics are well represented by the models. However, the models do not all match observations of OCS in mid and high latitudes, reflecting the variability of transport between models. Since this gas represents the main sulfur source in the mid-stratosphere, confidence in the rate of OCS oxidation and aerosol formation in the tropics is gained.
- SO_2 mixing ratios in the tropics show large variability between models. Model differences are probably due to the short lifetime of SO_2 in the tropics along with differences in the OH concentrations and transport differences.
- More SO_2 measurements would be valuable. Better knowledge of SO_2 concentrations in the UT would be required to obtain a correct description of the transport of sulfur into the stratosphere. Knowing SO_2 in the lower-mid stratosphere helps verify the OCS chemical destruction rate and the SO_2 to H_2SO_4 conversion rate, along with transport rates. Above 35 km, observations show an increase in SO_2 which can only be reproduced by models that include a photolytic conversion of gaseous H_2SO_4 into SO_2.
- Comparisons between models and satellite observations of aerosol extinction are generally fairly good at visible wavelengths but are less satisfactory for infrared wavelengths. Aerosol extinction measurements from SAGE II at 0.525 and 1.02 μm can be matched by models above 20-25 km altitude under nonvolcanic conditions. Tropical observations show a sharp vertical gradient in extinction at 17-20 km which varies with season and is not reproduced by the models. Models are less successful at reproducing extinction observations from the HALOE instrument at 3.46 and 5.26 μm.
- Models predict aerosol size distributions which can be approximated by a lognormal function except near regions of nucleation or evaporation. Integrated aerosol quantities such as surface area and effective radius can in principle be calculated without approximation from model size distributions, whereas satellite observations and in situ measurements by optical particle counters used to derive these quantities are either controlled by a priori assumptions regarding the size

distribution or have coarse resolution at the small size bins. Comparisons of these quantities during volcanically quiescent periods are problematic because much of the aerosol density may reside in particles too small to be observed, especially near nucleation regions.

- Simulations of the Mt. Pinatubo period are generally good but dependent on the assumed initial vertical distribution of volcanic sulfur. For instance, model results show very good agreement with column integrated lidar backscatter at both tropical and mid latitude sites, including the magnitude and timing of the aerosol maximum and the rate of decay. Comparisons with SAGE II extinctions show that models may under or over predict extinction at different altitudes depending on the applied model and the assumed vertical distribution of volcanic sulfur at the beginning of the event.
- The modeled rate of recovery from the Pinatubo eruption depends on the quantity considered (extinction, number density, surface area density) and the latitude and altitude of interest. Recovery time constants (e-folding times) show decay rates that lengthen with time past the eruption, consistent observations. Different models exhibit different recovery time constants, however, with a scatter not larger than that of the observations.

6.2 Scope and Rationale

The overall objective of this chapter is to assess whether transport of sulfur compounds (primarily SO_2 and OCS) from the troposphere and known physical processes can explain the distribution and variability of the stratospheric aerosol layer. Since aerosol models synthesize our knowledge about coupled aerosol processes, they, together with observations, are the main tools used here to test our current quantitative understanding of the processes controlling the formation and evolution of the stratospheric aerosol layer. The core of the chapter is devoted to detailed comparisons between global aerosol model simulations and observations. The observations and aerosol products derived from them are presented in Chapter 4. Comparisons are used to evaluate the performances of the models with respect to a range of relevant aerosol quantities and identify gaps in our understanding of aerosol processes or/and deficiencies in their representation in models and, where possible, assess problems in available data sets. It is worth stressing that this up-to-date modeling assessment is not a detailed model intercomparison. The use of different models provides a range of uncertainties in current model simulations, though true uncertainty is likely to be larger than the model spread. The models are described in detail in Section 6.3. They are all well-established global 2-D and 3-D aerosol-chemistry-transport models.

A number of questions which are discussed in the previous chapters are addressed in this up-to-date modeling assessment. The aerosol processes which are discussed in Chapter 1 are illustrated with examples from the models in Section 6.4. Section 6.5 presents direct comparisons between model simulations and measurements of gaseous precursors and aerosols for non-volcanic conditions. This allows us to evaluate the capabilities of global stratospheric aerosol models at the present time, in particular in reproducing the broad features of the non-volcanic aerosol layer. Continuous quiescent volcanic outgassing is considered a 'non-volcanic' source in the chapter as opposed to the intermittent explosive volcanic eruptions whose columns inject sulfur directly into the stratosphere. Sulfur budgets are derived and the respective contributions of OCS, SO_2, and particulate transported from the troposphere to the stratosphere are estimated. Sensitivity studies

designed to highlight model uncertainties and assess the extent to which changes in tropospheric concentrations of gaseous precursors (OCS, SO_2) and aerosols can affect the stratospheric distributions and trends of sulfate aerosols are described in Section 6.6.

Model simulations of a Pinatubo-like stratospheric sulfur injection are described in Section 6.7. They are evaluated against observations focusing on characteristics of the aerosol evolution such as the timing and magnitude of the peak aerosol loading and the aerosol decay rate. These simulations are compared with backscatter observations from lidar stations, satellite extinction measurements, and in situ measurements of particle number density. Finally, the overall results are discussed and summarized in Section 6.8. Model limitations and uncertainties due to the representation of transport and microphysics are discussed, along with limitations of the present observational data. Gaps in our understanding, along with recommendations for future observations and modeling work, are highlighted.

6.3 Model Descriptions

This section is devoted to the descriptions of the aerosol-chemistry-transport models used in the comparisons. Five different modeling groups participated in the comparisons for this chapter. Table 6.1 lists the participating models, investigators, and their institutions. References to each model are also given. Two of the models are three-dimensional (ULAQ, MPI), three are two-dimensional models (AER, UPMC, LASP). Each model represents the global domain from the surface to 30 km (MPI model) or 60 km (AER and UPMC) or higher (ULAQ AND LASP). Grid resolution ranges from 3.75^o to 10^o in latitude and from 1.2 km to 3.5 km in altitude, as detailed in Table 6.2. Model dynamics (wind fields and temperature) are calculated interactively in the UPMC and LASP 2-D models, but are specified from climatological analyses [Fleming et al., 1999] in the AER model. The MPI aerosol model is fully implemented within the Hamburg climate model ECHAM-4 GCM [Roeckner et al., 1996]. The ULAQ model used dynamical parameters taken from the output of a GCM. Tropospheric processes such as convection and cloud scavenging are included in the 3-D models, with time-dependent rates according to the GCM cloud processes. Two-dimensional models are not designed to simulate tropospheric dynamics or chemistry in detail, since topography, surface properties, and

Table 6.1: Participating Models

Model	Investigator	Institution	References
AER	D. Weisenstein	Atmospheric and Environmental Research, Inc. Lexington, MA, U.S.A.	Weisenstein et al., 1997 Weisenstein et al., 1998
UPMC	S. Bekki	University Pierre et Marie Curie Paris, France	Bekki and Pyle, 1992, 1993 Bekki, 1995
LASP	M. Mills	LASP, University of Colorado Boulder, CO, U.S.A.	Mills et al., 1999 Burkholder et al., 2000
MPI	C. Timmreck	Max-Planck Institut für Meteorologie Hamburg, Germany	Timmreck, 2001
ULAQ	G. Pitari	University L'Aquila Aquila, Italy	Pitari et al., 2002

Table 6.2: Model Domain and Resolution

Model	Type	Domain	Resolution	Dynamics
AER	2D	ground to ~ 60 km	9.5^o × 1.2 km	climatology
UPMC	2D	ground to ~ 60 km	9.5^o × 3.5 km	interactive
LASP	2D	ground to 112 km	5^o × 2 km	interactive
MPI	3D	ground to ~ 30 km	3.75^o(lon.) × 3.75^o(lat.) × 19 levels	GCM online
ULAQ	3D	ground to ~ 70 km	22.5^o(lon.) × 10^o(lat.) × 26 levels	GCM offline

localized emissions cannot be included. Therefore our approach in this report is to specify boundary conditions at the tropopause for the 2-D models so that inputs to the stratosphere will be as realistic as possible and independent of 2-D tropospheric dynamics.

Sulfur source gases may include SO_2, OCS, DMS, H_2S, and CS_2, as detailed in Table 6.3, but SO_2 and OCS are the only significant gas species in terms of sulfur input to the stratosphere. DMS, H_2S, and CS_2 have short lifetimes in the troposphere, yielding SO_2 which may be transported to the stratosphere. All models except MPI with an upper boundary at 30 km account for significant recycling of gaseous H_2SO_4 into SO_x (=S+SO+SO_2+SO_3) in the upper stratosphere [Rinsland et al., 1995] via photolysis. The rate of this photolysis reaction has been uncertain and therefore varies among the models, with most assuming photolysis in the UV, though recent work reports photolysis in the visible [Vaida et al., 2004; Mills et al., 2005]. This subject will be discussed further in Section 6.5.2. Most models allow changes in sulfur species to perturb the chemistry of

Table 6.3: Model Chemistry

Model	Source Gases	SO_x Species	$H_2SO_4 \rightarrow SO_2$	Rates from
AER	SO_2, OCS, DMS, H_2S, CS_2	SO_2, SO_3, H_2SO_4	yes	JPL-2000
UPMC	SO_2, OCS	S, SO, SO_2, SO_3, HSO_3, H_2SO_4	yes	JPL-2000
LASP	SO_2, OCS	SO_2, SO_3, H_2SO_4	yes	JPL-2000
MPI	SO_2, OCS, DMS	S, SO, SO_2, SO_3, HSO_3, H_2SO_4	no	JPL-2000
ULAQ	SO_2, OCS, DMS, H_2S, CS_2	SO_2, H_2SO_4	yes	JPL-97

OH and ozone, an important feedback during times of massive volcanic eruptions (i.e. larger than Pinatubo) [Bekki, 1995]. However, since OH concentrations are not significantly perturbed by the Pinatubo event, and O_3 concentrations, though perturbed, have a small effect on sulfur gases and aerosols, these feedbacks are not important to the results presented here. The MPI and AER model use pre-calculated values of OH and other oxidants, along with pre-calculated photolysis rates, derived from a model calculation with standard stratospheric chemistry. All the models employ reaction rates from JPL-97 [DeMore et al., 1997] or JPL-2000 [Sander et al., 2000].

The models used in this assessment were developed as stratospheric aerosol models. These models differ from tropospheric aerosol models in that resolving the size distribution of aerosol particles is crucial to predicting the correct sedimentation rate and therefore the lifetime of stratospheric particles. In the troposphere, only particles larger than ~ 1 μm settle appreciably, whereas the thinner air in the stratosphere causes sedimentation rates to be a strong function of both particle radius and air density. Even particles of 0.01 μm have significant sedimentation rates at 30 km. Tropospheric aerosol models typically deal only with total aerosol mass, but may assume a lognormal distribution to resolve the particle sizes. All the models here resolve aerosol sizes into sections, or "bins" (using a geometrical factor between the volumes of consecutive bins), with each bin size transported separately. These types of aerosol schemes are usually referred to as fully size-resolving aerosol schemes. Since the computational cost of resolving an additional dimension (i.e. size space) is very high, size-resolving schemes are only used in two-dimensional models and low-resolution global three-dimensional models.

Tropospheric aerosol models deal with many types of aerosols, including sulfate, dust, sea salt, organics, and black carbon. Stratospheric models typically deal with only sulfate particles (and PSC particles in polar regions), as the other particle types seldom penetrate the lowermost stratosphere. The sulfuric acid aerosols are treated as liquid binary solution droplets (or ternary solution droplets in polar regions). Their exact composition is directly derived from the surrounding temperature and humidity (and nitric acid concentration in polar regions) [Tabazadeh et al., 1997; Carslaw et al., 1995]. It has been suggested [Hunten et al., 1980; Cziczo et al., 2001] that meteoritic material may be contained in a significant fraction of stratospheric aerosols, but none of the models include meteoritic material because of the large uncertainty in its source and stratospheric abundance. The UPMC and ULAQ models include soot particles from surface sources, but find very little soot in the stratosphere due to efficient removal in precipitation. Tropospheric transport, including rapid transport in convective cells, is believed to play an important role in moving sulfur source gases from the boundary layer to the upper troposphere (see Chapter 2). Stratospheric models may not have the spatial resolution in the troposphere to resolve these localized transport features, or the localized nature of some sulfur sources, such as industrial SO_2 emissions. Two-dimensional models in particular have unrealistic tropospheres. This problem is addressed in this assessment by selecting tropopause boundary conditions for the 2-D models which are derived from either observations or 3-D models, so that the input of source gases and aerosols to the stratosphere will be as realistic as possible and less model-dependent.

Microphysical processes (nucleation, condensation/evaporation, coagulation, sedimentation) determine the evolution of the aerosol concentration in each size interval. Table 6.4 gives details of the size range and resolution used by each model. All but the

ULAQ model use volume doubling bin resolution. The ULAQ model uses radius doubling (or a factor of 8 in volume). Some models (UPMC, LASP, and ULAQ) account for different aerosol composition in cold polar regions, where HNO_3 and H_2O condense onto particles forming polar stratospheric clouds (PSCs). Because this report is not intended to be an assessment of PSCs, we have not performed model comparisons with observations when PSCs are present. The presence of PSCs, however, will impact the lifetime of sulfate particles in polar regions.

For details of each model's microphysical scheme, refer to the publications listed in Table 6.1. Here we mention only major similarities and differences. The UPMC model employs heterogeneous nucleation only, the AER, LASP, and MPI models use only homogeneous nucleation, and the ULAQ model uses both homogeneous and heterogeneous nucleation. Nucleation theories and observations often differ by several orders of magnitude, so there is much uncertainty in this calculation. The details of the nucleation scheme are probably less important than correctly predicting regions where nucleation occurs (mainly the tropical tropopause and polar regions). Coagulation will reduce number densities when nucleation rates are large, so large differences in nucleation rates between models do not translate into large differences in predicted size distributions. See Section 6.6.1 for more discussion of this topic.

The processes of condensation and evaporation, coagulation, and sedimentation are treated similarly in all the models though details of the implementations are different. Rainout and washout remove aerosol particles from the troposphere and act as the major sink for stratospheric aerosols in the models. These processes vary with time in the 3-D models but are parameterized more simply in the 2-D models.

Table 6.4: Aerosol Schemes

Model	# bins	Size Range	Resolution	Composition
AER	40	0.00039 to 3.2 μm	volume doubling	H_2SO_4/H_2O
UPMC	25	0.01 to 2.5 μm	volume doubling	$H_2SO_4/H_2O/HNO_3$/soot
LASP	45	0.0005 to 10 μm	volume doubling	$H_2SO_4/H_2O/HNO_3$
MPI	35	0.001 to 2.58 μm	volume doubling	H_2SO_4/H_2O
ULAQ	11	0.01 to 10.2 μm	radius doubling	$H_2SO_4/H_2O/HNO_3$/soot

6.4 Model Illustrations of Aerosol Microphysics

In the present section, we illustrate the stratospheric aerosol lifecycle discussed in Chapter 1 with examples from the models. As shown in Figure 6.1, the nucleation process occurs year-round in the tropopause region within the AER model when the Vehkamäki et al. [2002] nucleation parameterization is applied. Between 30°N and 30°S, nucleation occurs from about 10 to 18 km in altitude, though the midlatitude tropopause experiences nucleation to a lesser extent and in a narrower altitude region. The maximum nucleation rate is 2-3 km below the tropopause in the tropics, with 90% of model nucleation

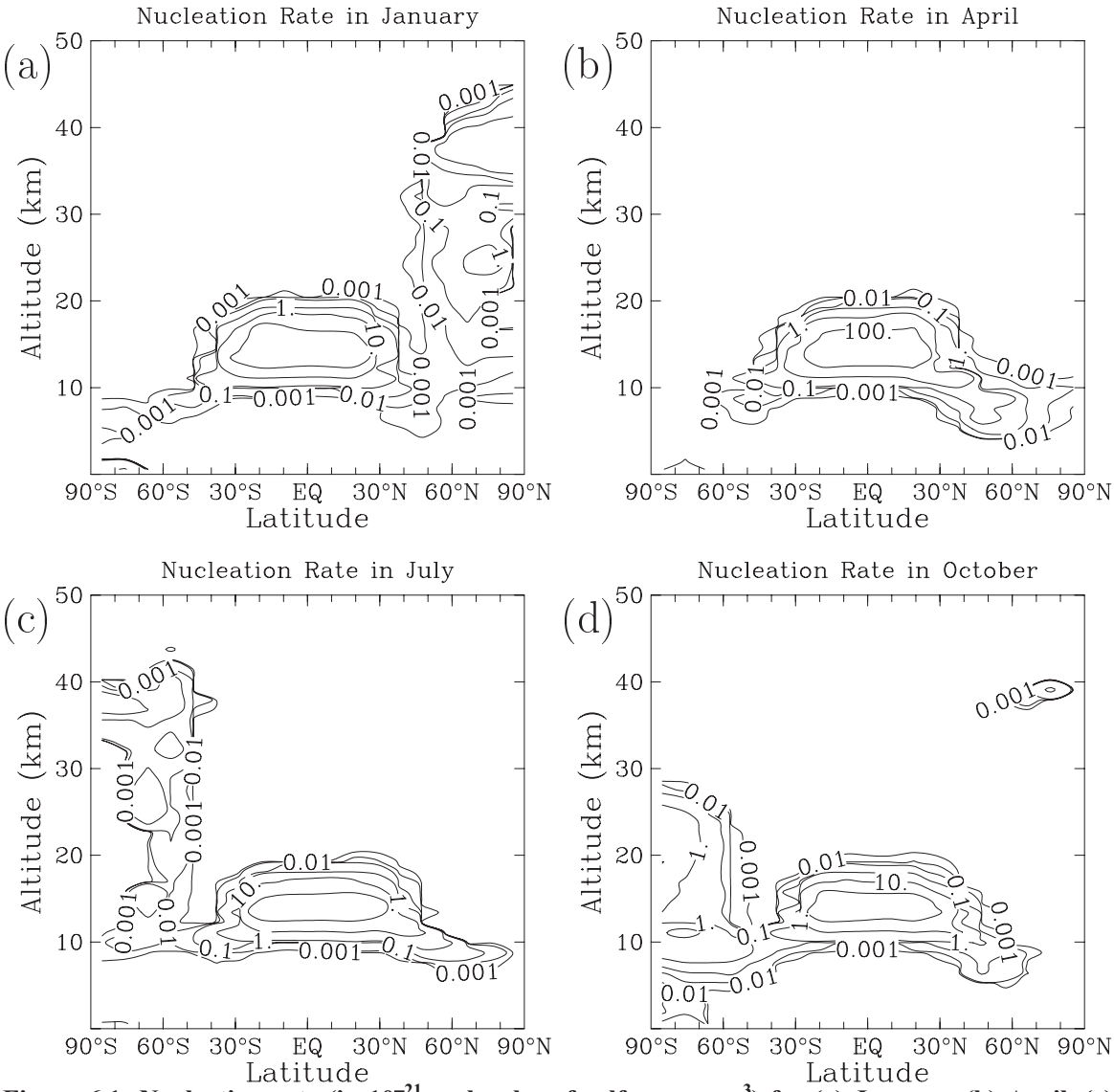

Figure 6.1: Nucleation rate (in 10^{-21} molecules of sulfur per cm^3) for (a) January, (b) April, (c) July, and (d) October as calculated by the AER 2-D model using the Vehkamäki et al. [2002] nucleation scheme. Contours are 0.0001, 0.001, 0.01, 0.1, 1, 10, 100.

occurring in the troposphere. The freshly-nucleated particles are transported into the stratosphere, the imposed primary aerosol merely contributing to the larger size range. The freshly-nucleated particles contribute only a minor amount of aerosol mass to the stratosphere, but are important in determining number density and particle size distribution. The high latitudes experience nucleation in winter (November to March in the Northern Hemisphere, May to November in the Southern Hemisphere) from the tropopause to 30 or even 45 km.

It should be noted that nucleation in the real atmosphere is episodic; occurring in limited geographical regions in short bursts when convection brings high concentrations of gaseous H_2SO_4 into the upper troposphere, or when wave activity depresses local temperatures and causes supersaturation. The models do not include the necessary geographical resolution or convective and wave activity to stimulate nucleation bursts, and therefore tend to calculate nucleation at slower rates continuously over large

geographical areas and time periods. A more accurate representation of nucleation processes within large-scale models would require subgrid scale parameterizations accounting for small-scale fluctuations in key parameters (temperature, sulfuric acid, water vapor, preexisting particles). Because bursts of nucleation would produce extremely high particle concentrations in localized areas, coagulation would be very effective in reducing number concentration within days to weeks. Since coagulation of nanometer-sized particles is self-limiting, it is expected that, for global modeling, simulating the temporal variation of nucleation rate is less important than predicting correctly where and in what seasons nucleation occurs.

Some simple time-dependent microphysical box model calculations will illustrate the processes of nucleation, coagulation, condensation, sedimentation, and evaporation. These calculations with the AER model use 150 bins over the size range from 0.4 nm to 3.2 μm and a time step of 3.6 seconds to deal with rapid aerosol evolution. The AER model's usual time step is 1 hour with 40 bins. Coagulation is active in all simulations, but is generally ineffective when number concentrations are low.

Figure 6.2 shows the evolution of the aerosol particle size distribution over the course of 10 days, assuming no aerosol removal by sedimentation, for typical upper tropospheric conditions (124 mb, 199 K, H_2O mixing ratio of 3.14 ppmv or 14% relative humidity). The calculations are initialized with 40 pptv of H_2SO_4 in the gas phase and no aerosol particles. Condensation is ignored in these calculations so that the effects of nucleation and coagulation are evident. In Figure 6.2a, all the initial gas phase H_2SO_4 is nucleated within the first second, and the distribution subsequently evolves by coagulation. Figure 6.2b represents a case with the same initialization, but including a continuous source of gas phase H_2SO_4 of 40 pptv/day, causing nucleation throughout the integration. The size distributions shown are indicative that an air parcel has seen a recent nucleation event.

The process of heteromolecular condensation is illustrated in Figure 6.3 under lower stratospheric conditions (27.8 mb, 216.5 K, H_2O mixing ratio of 2.76 ppmv or 0.3%

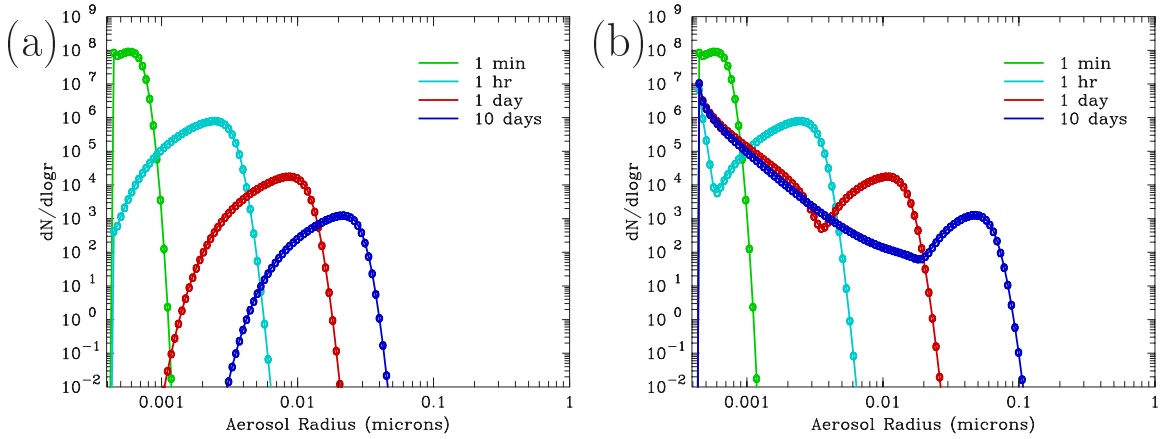

Figure 6.2: Evolution of calculated aerosol size distribution using a microphysical box model for typical upper tropospheric conditions (124 mb, 199 K, H_2O mixing ratio of 3.14 ppmv or 14% relative humidity). Panel A initializes the model with 40 pptv of H_2SO_4 in the gas phase and no aerosol particles. Panel B represents a case with the same initial H_2SO_4 concentration, and a continuous source of gas phase H_2SO_4 of 40 pptv per day. The model uses 150 bins over the size range from 0.4 nm to 3.2 μm and a time step of 3.6 seconds. In this computation, nucleation and coagulation are the only processes responsible for the aerosol evolution, as condensation and sedimentation have been ignored.

relative humidity). The model is initialized with 40 pptv of H_2SO_4 in the gas phase and 40 pptv of H_2SO_4 as aerosol particles with a mode radius of 0.08 μm and includes a continuous source of gas phase H_2SO_4. Figure 6.3a shows a case with nucleation switched off and hence condensation of H_2SO_4 occurs on the preexisting aerosols. Condensation and coagulation strongly reduce the number of small particles while increasing the number of larger particles. As a result, the size distribution narrows. Figure 6.3b shows a case with nucleation included and a continuous source of gas phase H_2SO_4 of 40 pptv/day. The nucleation burst within the first minute provides an additional surface for condensation, and the particles grow rapidly, with most of the condensation occurring on the smaller nucleation-mode particles rather than the initial larger mode. Coagulation is not very effective in case (a) because of the low number densities, but is effective in case (b).

The process of sedimentation is illustrated in Figure 6.4, which shows the evolution over 10 days of a model-calculated aerosol size distribution initialized with a wide lognormal distribution and no gas phase H_2SO_4. In this case study, aerosol particles are assumed to be lost when they sediment by 100 m; particles are not replaced by sedimentation from above. Figure 6.4a shows a calculation at 40 mb (~ 22 km) and Figure 6.4b a calculation at 6.2 mb (~ 35 km). The dependence of sedimentation rate on air density is seen. The larger particles in the distribution are removed at a faster rate at higher altitudes. Even mid-sized particles (r ~ 0.05 μm), which have negligible sedimentation velocity in the lower stratosphere, experience substantial sedimentation in the upper stratosphere. The global effect of sedimentation is redistribution of sulfur mass from the middle stratosphere to the lower stratosphere, where subsequent transport of particles into the troposphere leads to removal. This is illustrated in Figure 6.5, which shows calculated vertical profiles of total sulfur (= OCS + SO_2 + gas-phase H_2SO_4 + condensed H_2SO_4) from the AER model with and without sedimentation at the equator under annual average conditions. Without sedimentation, the vertical profile of total sulfur is, as expected, almost constant with altitude throughout the stratosphere. With sedimentation, the total

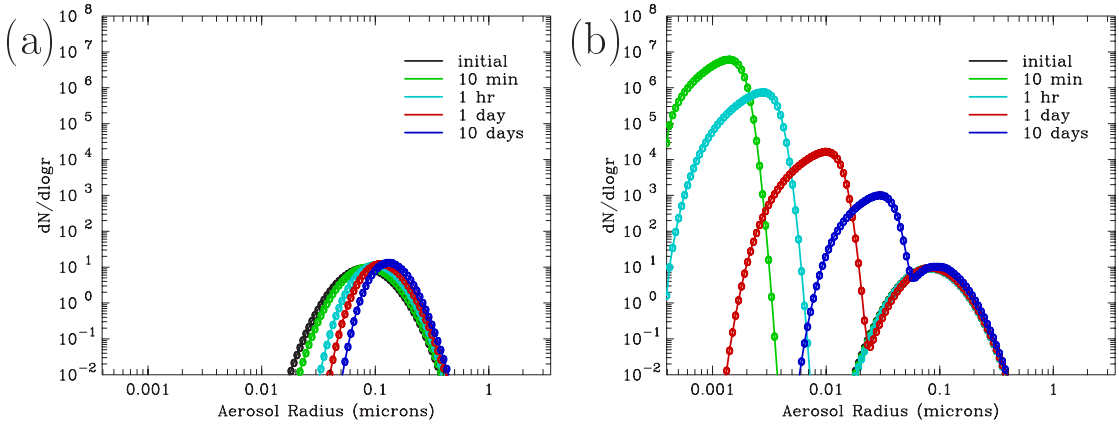

Figure 6.3: Evolution of calculated aerosol size distribution using a microphysical box model for typical lower stratospheric conditions (27.8 mb, 216.5 K, H_2O mixing ratio of 2.76 ppmv or 0.3% relative humidity). The model is initialized with 40 pptv of H_2SO_4 in the gas phase and 40 pptv of H_2SO_4 as aerosol particles with a mode radius of 0.08 μm and includes a continuous source of gas phase H_2SO_4 of 40 pptv per day. In Panel A, only condensation onto the preexisting particles is allowed to occur, along with coagulation. In panel B, an initial burst of nucleation creates small particles, which then grow by condensation and coagulation. Sedimentation is disabled. The model uses 150 bins over the size range from 0.4 nm to 3.2 μm and a time step of 3.6 seconds.

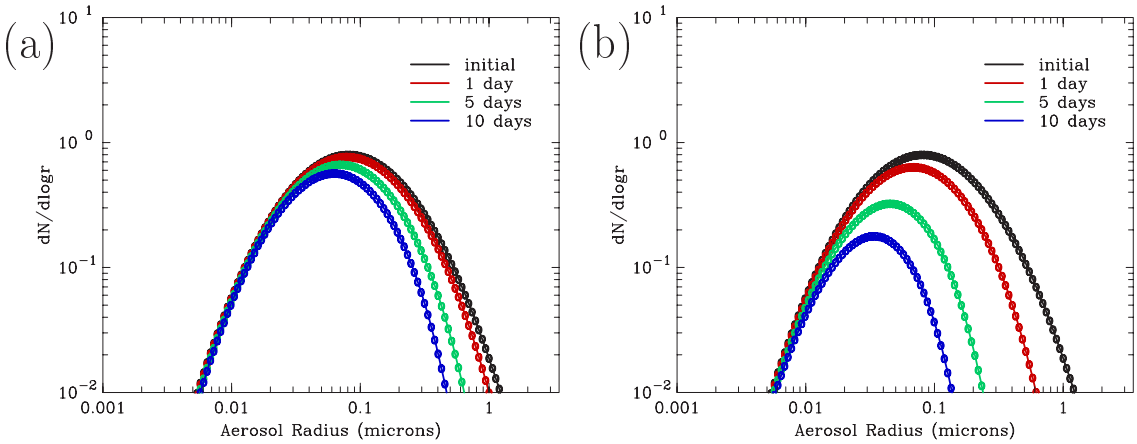

Figure 6.4: Evolution of calculated aerosol size distribution over 10 days using a microphysical box model to illustrate the sedimentation process at (a) 40 mb and (b) 6.2 mb. The model is initialized with no H_2SO_4 in the gas phase and 1.27×10^{15} molecules/cm^3 of H_2SO_4 as aerosol particles. Sedimentation is assumed to occur when particles fall by 100 m; particles are not replaced by sedimentation from above. The model uses 150 bins over the size range from 0.4 nm to 3.2 μm and a time step of 3.6 seconds.

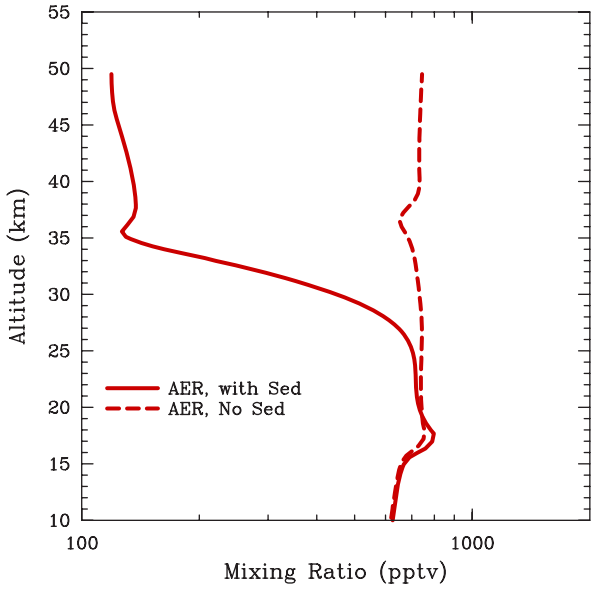

Figure 6.5: Vertical profiles of annual average total sulfur at the equator as calculated by the AER model with (solid line) and without (dashed line) sedimentation.

sulfur decreases with increasing altitude in the lower and middle stratosphere. In the upper stratosphere, where all sulfur is in the gas phase (above the aerosol layer), there is no sedimentation and therefore the profile is constant with altitude. Vertical redistribution of sulfur by sedimentation is very effective. Indeed, the total sulfur above the aerosol layer is less than 150 pptv with sedimentation whereas it is of the order of 700 pptv without sedimentation. Total condensed sulfur in the stratosphere is, however, only 12% less with sedimentation than without.

In the upper stratosphere, particles also experience evaporation. Figure 6.6 illustrates this process at a pressure of 3.2 mb (~ 40 km) and temperature of 255 K. The model is initialized with 90 pptv of H_2SO_4 in the gas phase which remains constant throughout the integration and 150 pptv of H_2SO_4 as aerosol particles, simulating a situation in which an aerosol distribution is moved instantaneously from 35 to 40 km and evaporates, its

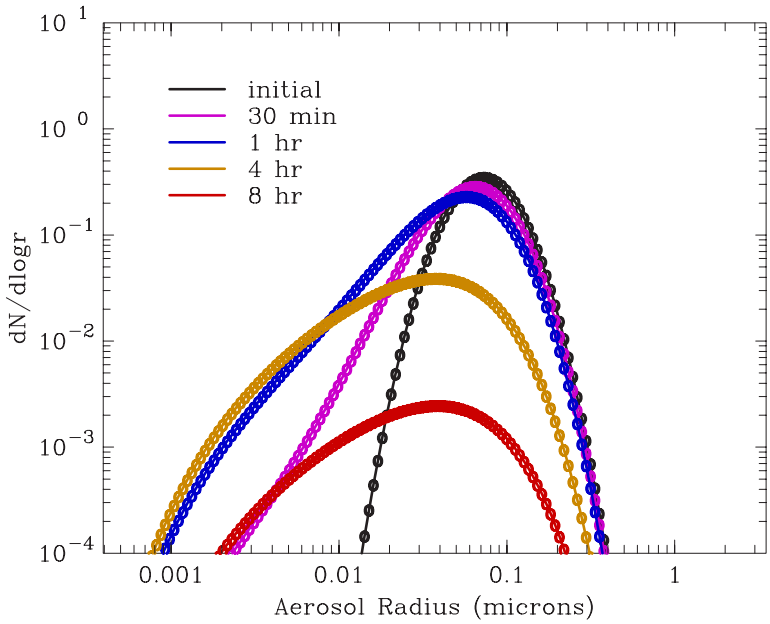

Figure 6.6: Evolution of calculated aerosol size distribution over 8 hours using a microphysical box model to illustrate the evaporation process at 3.2 mb and 255 K. The model is initialized with 90 pptv of H_2SO_4 in the gas phase which remains constant throughout the integration and 150 pptv of H_2SO_4 as aerosol particles. The model uses 150 bins over the size range from 0.4 nm to 3.2 μm and a time step of 3.6 seconds.

evaporation not perturbing ambient conditions. Sedimentation is disabled for clarity. The initial size distribution is lognormal, but as the particles evaporate, particles decrease to smaller sizes than in the initial distribution, and the shape of the distribution changes. In our example, the number of particles does not change for the first hour despite rapid evaporation. All particles are essentially evaporated within one day.

In the atmosphere, particles are transported as they grow by condensation and coagulation, and mixed with particles of different ages. The result is the size distributions produced in a global model. Figure 6.7 shows calculated size distributions from the AER 2-D model at the equator and 47°N in April under nonvolcanic conditions. At the equator, the transport moves particles upward and polewards, though mixing also brings aged particles from higher latitudes into the tropical lowermost stratosphere. In general, particles age as they ascend in the tropics. The peak of small particles (< 0.001 μm) at 18 km is a result of nucleation in the tropical upper troposphere and lower stratosphere, whereas the larger particles are those which have resided in the stratosphere for some time. At higher altitudes (23 and 27 km), only the large mode remains with maximum number density at about 0.1 μm, as the small particles have been removed by coagulation. In the upper stratosphere at 32 and 37 km, evaporation has produced particles smaller than 0.01 μm. At 47°N, the 18 km level shows some effects from nucleation near the tropopause. At higher altitudes, the main influence is downward transport from regions where evaporation and sedimentation have depleted the particle densities. Figure 6.8 shows calculated aerosol size distributions at 76°N in February and August. Winter polar conditions lead to nucleation at all altitudes in the middle stratosphere in February. Condensation rates at high latitudes are most pronounced at high altitudes where aerosol-free air flows from above into the polar vortex. In August at 76°N, the size distribution contains a single mode, with peak number density at greater radii at lower altitudes, reflecting the strong downward transport and associated particle aging. The aged size

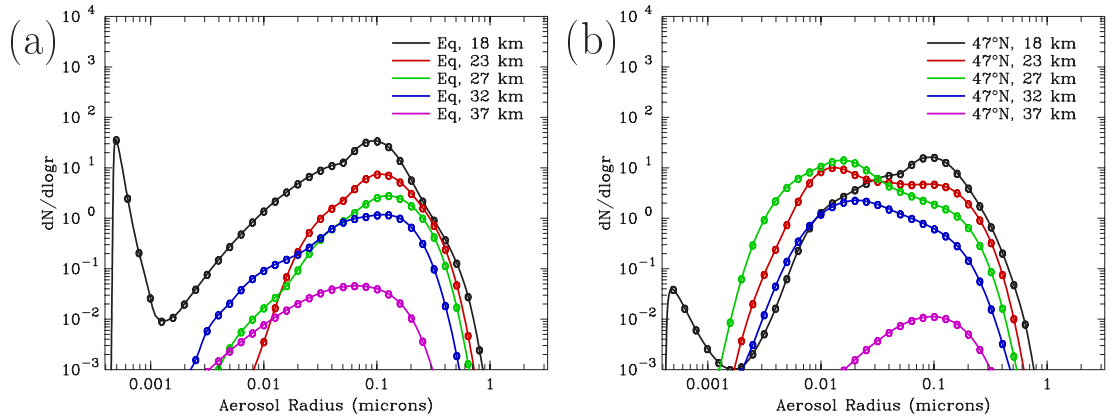

Figure 6.7: Calculated aerosol size distribution from the AER 2-D model in April at (a) the equator and (b) 47°N. The model uses 40 bins over the size range from 0.4 nm to 3.2 μm and a time step of 1 hour.

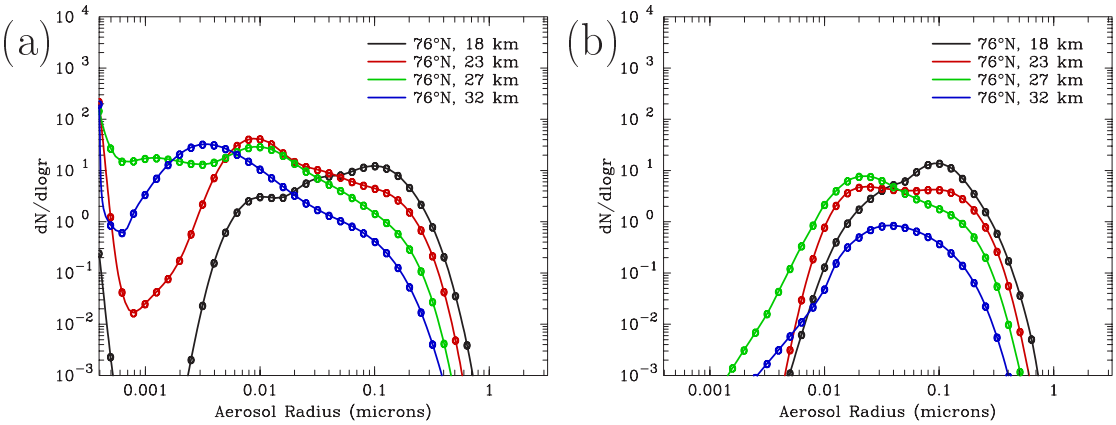

Figure 6.8: Calculated aerosol size distribution from the AER 2-D model at 76°N in (a) February and (b) August. The model uses 40 bins over the size range from 0.4 nm to 3.2 μm and a time step of 1 hour.

distributions resemble a lognormal distribution, which corroborates the use of this functional form for the simplified description of size distributions in Chapters 4 and 5. However, it must be clear that this remains an approximation, limitations of which have been addressed in Chapter 4.

6.5 Model Simulations of Nonvolcanic Conditions

6.5.1 Description of Calculations

The goal of these simulations is to model the stratospheric aerosol layer under nonvolcanic conditions. This will test our understanding of sulfur source gas emissions and transport, and chemical and microphysical processes. Comparisons will be made to observational data taken during volcanically quiescent years. To simplify the comparisons, the models all used identical boundary conditions for OCS and the 2-D models used identical boundary conditions for SO_2. Each model was run for multiple years until an annually-repeating state was reached.

Details of OCS sources and sinks are discussed in Chapter 2, Section 2.3.1. But because of the long lifetime of OCS, its concentration in the upper troposphere is fairly constant. Therefore we employ constant mixing ratio boundary conditions in the models. The OCS mixing ratio at the surface was specified as 512 pptv with no seasonal or spatial variation,

based on northern hemisphere annual averages reported in Bandy et al. [1992]. The MPI model doesn't calculate OCS but prescribes the mixing ratio with monthly mean values from a 2-D simulation [Grooss et al, 1998]. Seasonal variability of OCS near the tropopause is of order 1% or less in all models. The 3-D models used estimates of SO_2 emission sources from IPCC [Houghton et al., 2001] and allowed model transport by convection and the general circulation to determine SO_2 at the tropical tropopause. Resulting tropopause SO_2 mixing ratios were 25-37 pptv (annual average 30 pptv) in the ULAQ model and 8-13 pptv (annual average 10 pptv) in the MPI model. The two-dimensional models used specified boundary conditions for SO_2 at the tropical tropopause. Since tropopause SO_2 data was not available, we used results from the three-dimensional tropospheric aerosol models which participated in the *IPCC* climate assessment report [Houghton et al., 2001]. The mean annual average value of tropopause SO_2 over the 11 models averaged from 20^oS to 20^oN was 38.9 pptv [J. Penner, personal communication]. We adopted 40 pptv as the tropical tropopause SO_2 boundary condition, with a range of 0 to 80 pptv for sensitivity studies. The 2-D models, unlike the 3-D models, had no seasonal variation in tropopause SO_2.

The ULAQ 3-D model deals with both tropospheric and stratospheric aerosol particles, including interactions between soot, organics, sea salt, and sulfate particles. The MPI 3-D model treats only sulfate aerosols, and performs microphysical calculations only in the stratosphere and upper troposphere, treating only bulk sulfate mass below. For the 2-D models, we impose a primary aerosol concentration and size distribution at the tropical tropopause, based on aircraft observations made by the University of Denver Aerosol Group (S.-H. Lee, personal communication) using the Focused Cavity Aerosol Spectrometer (FCAS) instrument [Jonsson et al., 1995] between July 1996 and October 1999. This instrument, which is a single particle optical aerosol spectrometer, is discussed in Chapter 3, Section 3.4.3. The 475 size distributions were measured between 18°S latitude and 1.8°N latitude and at potential temperatures between 390 K and 420 K. In 314 cases, the location of the tropopause was known and the distance above the tropopause ranged from -0.43 km to 2.67 km with the mean value being 1.46 km above the tropopause. Only 10 size distributions of the 314 cases were known to be below the tropopause. Thus, the vast majority of the particles sampled for this characterization are believed to consist primarily of sulfate, based on their measurement location [Murphy et al., 1998]. The sizes reported here are those observed at the laser of the FCAS after the particles have undergone heating which removes much of the water from the sulfate. Size distributions were recorded in 32 size channels, with channel mean diameters covering the range from 0.064 μm to 3.12 μm. Each distribution was normalized to a common total sulfate concentration and then the distributions averaged. Figure 6.9 shows the observed distributions and the mean used as the tropopause boundary condition in the 2-D model calculations presented in this chapter. The mean sulfate mass mixing ratio for the 475 measurements was 0.258 ppbv (0.854 ppbm) and the standard deviation of this value was 0.049 ppbv (0.162 ppbm). We adopted the mean value for our tropopause boundary condition, with two standard deviations defining upper and lower limits for sensitivity. As a further sensitivity, we also assume no primary aerosols in the measured size range at the tropopause, allowing the models to generate particles in the upper troposphere which are transported into the stratosphere.

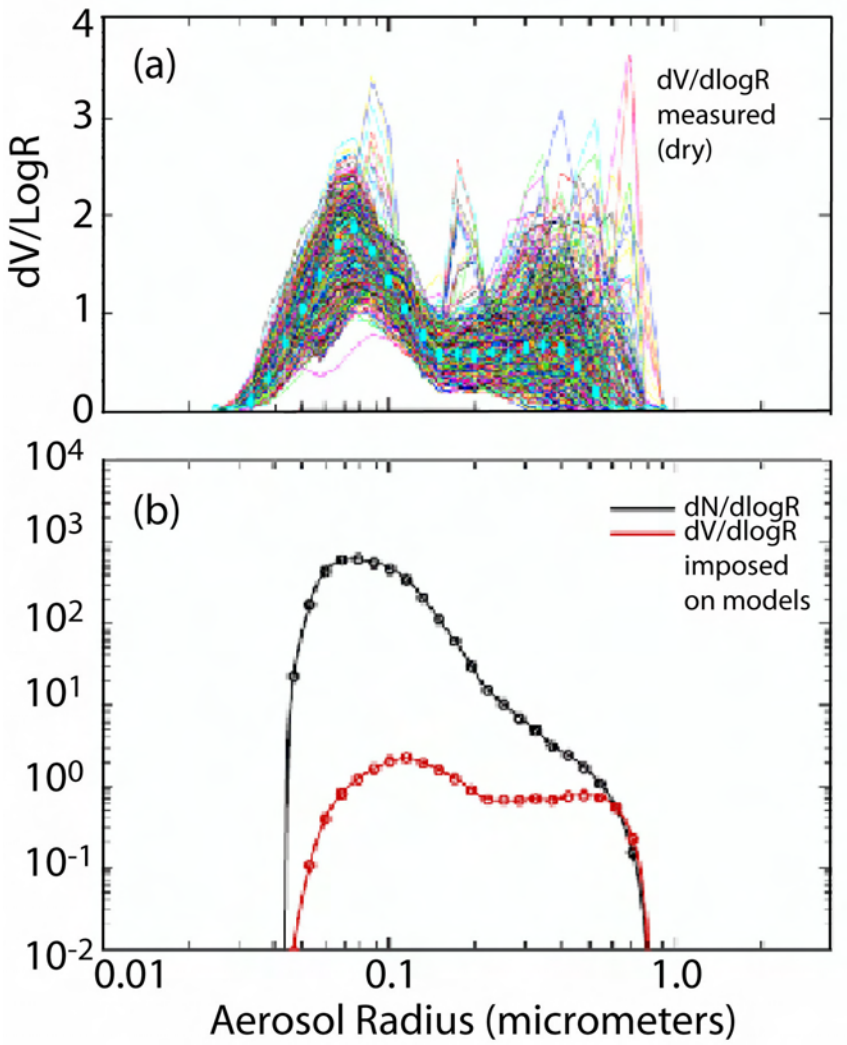

Figure 6.9: Size distribution near the tropical tropopause (a) observed by the FCAS instrument [Jonsson et al., 1995] as a dry volume distribution (dV/dlogR) along with the observational mean (heavy line) and (b) number and volume size distribution (dN/dlogR, dV/dlogR) at the tropical tropopause after hydration used as the tropopause boundary condition in the model calculations. Each observational profile was normalized to the same sulfate mass. Figure (a) provided by J.C. Wilson and S.-H. Lee (private communication).

6.5.2 Comparisons to Precursor Gas Measurements

The model-calculated OCS is compared to observations from the Atmospheric Trace Molecule Spectroscopy (ATMOS) experiment on the space shuttle in 1994 (ATLAS-3) [Gunson et al., 1996; Rinsland et al., 1996] and from the MkIV Fourier transform infrared spectrometer balloon-borne instrument [Leung et al., 2002] between 1992 and 2000. Figure 6.10a shows model-data comparisons with ATMOS at 5°N in November of 1994. The model results are all generally within the error bars of the measurements at 5°N and below 26 km. The ULAQ model has higher OCS concentrations (by 20-30 pptv) in the lower stratosphere than the other models because of OCS production from CS_2 in the mid to upper troposphere, which augments the 512 pptv of OCS specified at ground level. Note that some of the 2-D models also contain this source of OCS, but without effective convection it does not impact the stratosphere as strongly. The good model-measurement agreement in the tropics is reassuring because this region is where tropospheric source gases enter the stratosphere and where the major chemical loss of OCS occurs.

Figure 6.10b shows model comparisons with MkIV observations of OCS at 65°N in July. Additional plots showing comparisons at other latitudes are found in the supplementary material at http://www.sparc.sunysb.edu. The models show more variability in mid and high latitudes than in the tropics. This is a result of variations in model transport rates as OCS is transported from low to higher latitudes in the mid stratosphere. All models are generally within the error bars at 35°N. At 65°N in July, the LASP model simulation is sometimes too low and the MPI and ULAQ simulations sometimes too high in comparison with the MkIV limited observations. Correlations between OCS and other long-lived tracers would be most appropriate for testing the rate of chemical destruction of OCS independent of a particular model's transport.

The only available measurement of SO_2 in the stratosphere under nonvolcanic conditions is one ATMOS profile taken in April of 1985 [Rinsland et al., 1995]. Comparison of this

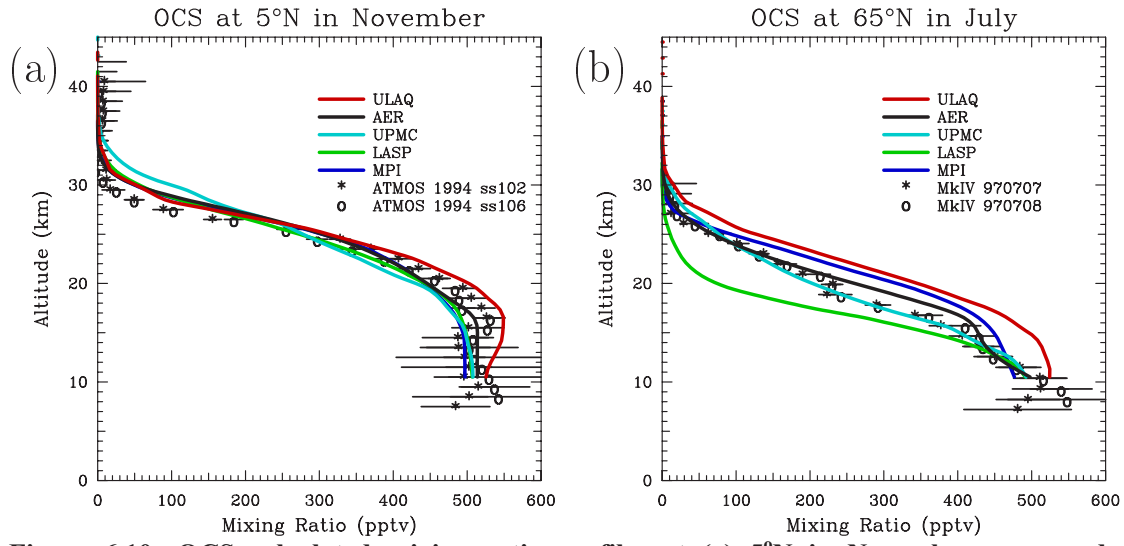

Figure 6.10: OCS calculated mixing ratio profiles at (a) 5°N in November compared to ATMOS observations [Gunson et al., 1996; Rinsland et al., 1996] and (b) 65°N in July compared to MkIV balloon observations [Leung et al., 2002].

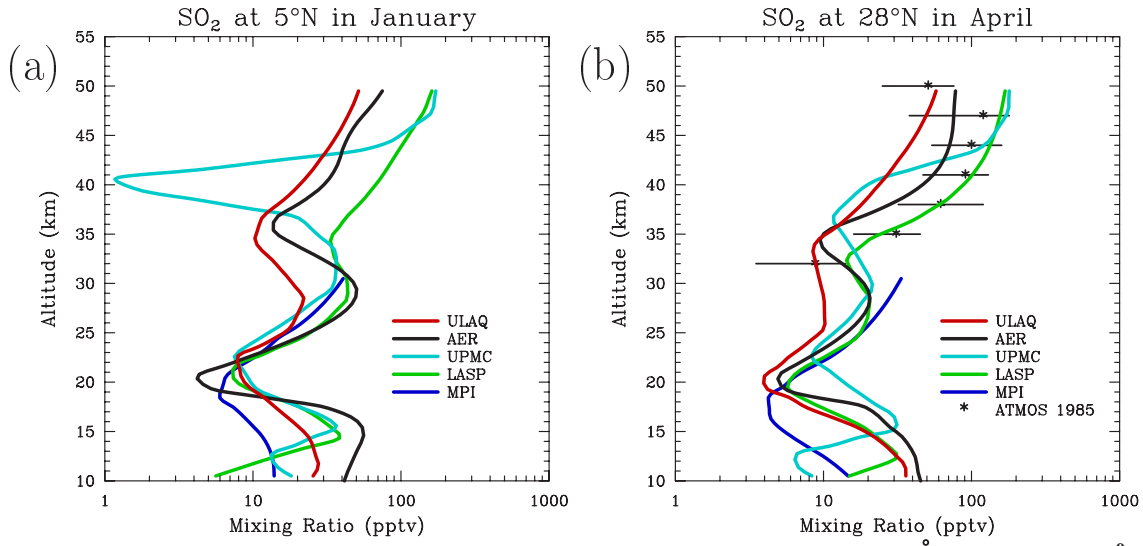

Figure 6.11: Model-calculated SO_2 mixing ratio profile (a) for January at 5°N and (b) at 28°N in April from model calculations and ATMOS observations taken in 1985 [Rinsland et al., 1995].

profile with model results at 28°N is shown in Figure 6.11b. Figure 6.11a shows a similar plot at 5°N in January for model results only. The 2-D models have imposed SO_2 concentrations of 40 pptv at the tropopause (~ 16 km). The 3-D models calculate about 25 pptv (ULAQ) and 10 pptv (MPI) at the tropopause at 5°N in January. Model profiles of SO_2 show falling concentrations from the surface to 20 km due to chemical conversion of surface-emitted SO_2. Photodissociation of OCS causes rising SO_2 concentrations between 20 and 30 km. The sharp rise in SO_2 concentrations above 35 km is a result of aerosol evaporation releasing H_2SO_4 into the gas phase, which is then photolyzed to give back SO_2. The model results do not agree well with each other, varying by factors of 5. Only the LASP model is a close match to the ATMOS observations between 35 and 47 km, with the UPMC model also agreeing with observations between 42 and 47 km. The AER and ULAQ models are lower than observations in most of this altitude range, while the MPI model does not extend high enough for comparison. Additional intercomparisons among the models at 5°N, 45°N, and 45°S for January and July are shown in the supplementary material. As with OCS, model agreement is better in the tropics than at higher latitudes. Intermodel differences in SO_2 in the tropics are much larger than for OCS, a result of the much shorter lifetime of SO_2 and differences in OH concentration.

The sharp rise in SO_2 concentrations above 35 km (Figure 6.11) is a result of aerosol evaporation releasing H_2SO_4 into the gas phase, which is then photolyzed to give back SO_2. The rate of this photolysis reaction has been uncertain until recently and thus varies among the models, with most assuming photolysis in the UV. The UPMC model shows very low SO_2 concentrations at 40 km because the sulfur exists as H_2SO_4 there. A recent paper reports photolysis in the visible [Vaida et al., 2004]. Mills et al. [2005] applied visible H_2SO_4 photolysis in a microphysical model and compared results with observations of H_2SO_4, SO_3, and SO_2 [Arnold et al., 1981; Reiner and Arnold, 1997; Schlager and Arnold, 1987; Viggiano and Arnold, 1981; Rinsland et al., 1995] between 30 and 50 km. They found that an additional upper stratospheric loss mechanism was required to explain vertically decreasing H_2SO_4 and SO_3 vapor above 40 km. Loss of H_2SO_4 by neutralization by metals on meteoritic dust, which acts as a permanent sink for sulfur, was found to be consistent with observations. Photolysis of H_2SO_4 to SO_2 in this region preserves gaseous sulfur in the upper stratosphere. SO_2 is transported downward into the polar regions where it reacts with OH in the presence of sunlight to regenerate H_2SO_4 and then condenses into sulfuric acid aerosols. During polar night, SO_2 will remain in the descending air due to lack of OH. At the return of sunlight in springtime, a descending and growing aerosol layer has been observed [Hofmann et al., 1989], consistent with the model calculations.

6.5.3 Calculated Aerosol Budgets and Burdens

The models can provide detailed descriptions of sulfur species in the stratosphere, their burdens, fluxes across the tropopause, and chemical and microphysical transformation rates. While we cannot specifically validate most of these values against observations, we do gain confidence in them knowing that OCS concentrations reasonably represent observations, and that calculated aerosol extinctions compare favorably with satellite measurements under nonvolcanic conditions. Figure 6.12 diagrams the stratospheric sulfur budget calculated by the AER model. Aerosol accounts for 39% of the total sulfur mass of the stratosphere, with OCS accounting for 58% and SO_2 for 2%. CS_2, DMS, and H_2S have short tropospheric lifetimes and only insignificant amounts of these species are found in the stratosphere. Sulfuric acid gas is continually produced by oxidation of SO_2,

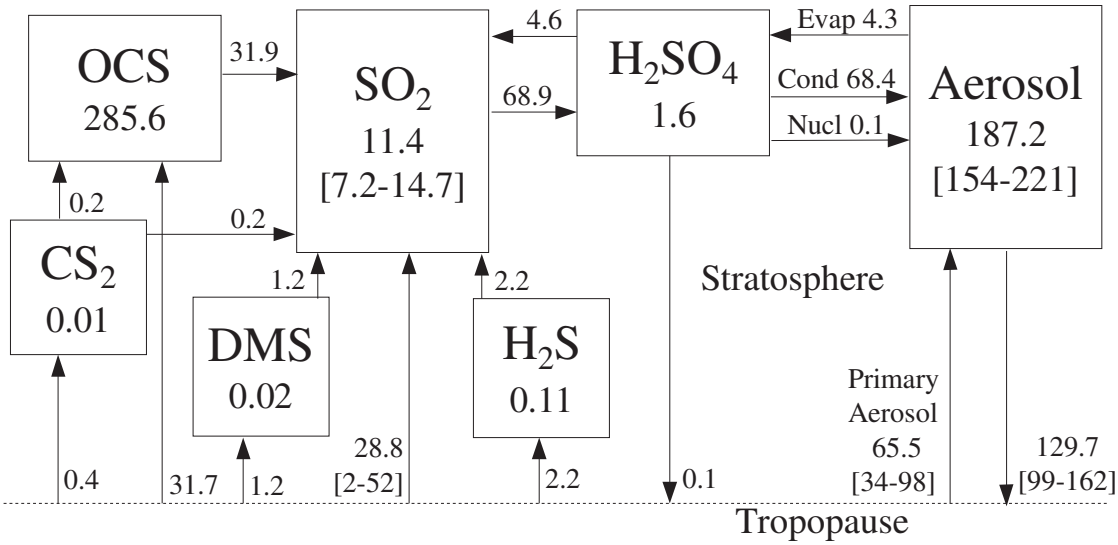

Figure 6.12: Stratospheric sulfur budget as calculated by the AER model. Burdens are in units of 10^9 grams of sulfur, fluxes and chemical transformation rates in 10^9 grams of sulfur per year. Values in square brackets represent a range derived from sensitivity studies as detailed in the text. Rates of the microphysical processes of nucleation (Nucl), condensation (Cond), and evaporation (Evap) are also shown.

but in the lower and middle stratosphere it quickly condenses into aerosol. In the upper stratosphere above about 35 km, aerosols evaporate to release sulfuric acid gas. Some of the H_2SO_4 gas at these levels photolyzes into SO_2.

The cross-tropopause fluxes shown in Figure 6.12 represent net annual fluxes across the seasonally-varying tropopause. The range shown for SO_2 (2 to 52 kilotons per year) is from sensitivity studies imposing 0, 40, or 80 pptv of SO_2 at the tropical tropopause. In addition, 65.5 kilotons of sulfur per year is transported to the stratosphere in primary aerosol particles when imposing the S.-H. Lee (personal communication) mean particle mass density at the tropical tropopause (34-98 kT/yr range over two standard deviations). Without this imposed particle flux, the AER model would calculate a sulfur flux to the stratosphere of 24 kT/yr in particles and a stratospheric aerosol burden of 145 kT of sulfur. Flux values are highly model-dependent, being the product of transport rate and tropopause concentration. In the AER model, 25% of sulfur transported to the stratosphere is in the form of OCS, 22% in the form of SO_2, 3% as other source gases, and 50% as aerosol. The particle contribution could range from 27% to 60%. In the ULAQ 3-D model [Pitari et al., 2002], 43% of the stratospheric particulate sulfur comes from OCS, 27% from SO_2, and 30% from particles transported across the tropopause.

Chemical transformation rates show that stratospheric SO_2 is produced almost entirely from OCS dissociation if transport from the troposphere is small. But with the assumption of 40 pptv of SO_2 in the TTL, roughly equal amount of SO_2 come from transport and OCS. The global mean model-calculated lifetime of OCS against chemical loss in the stratosphere is 9 years. The mean stratospheric lifetime of SO_2 due to OH destruction is two months, though the local lifetime in the middle stratosphere is often 40 days or less. OCS dissociates primarily above 25 km, while SO_2 transported from the troposphere remains in the lowermost stratosphere. OCS is responsible for most of the SO_2 above 20 km, and cross-tropopause transport is responsible for a large fraction below this altitude. Both condensation and nucleation transform gas phase H_2SO_4 to aerosol, but condensation represents 99.8% of the total gas-to-particle transformation. Transport of primary aerosol from the troposphere may represent an input of stratospheric aerosol

equivalent to the stratospheric sulfate condensation. The lifetime of aerosol in the stratosphere is about 1.4 years according to the AER model. If OCS were the only source of stratospheric sulfur, the aerosol lifetime would be 2.5 years. If SO_2 were the only source of stratospheric sulfur (OCS omitted from model calculation), the lifetime would be 1.2 years. This model-derived budget of stratospheric sulfate indicates that cross-tropopause flux of SO_2 and primary aerosol may be large contributors to the stratospheric aerosol burden, but large uncertainties remain in quantifying that flux. Comparisons with satellite extinction observations will be helpful in reducing this uncertainty.

The morphology of stratospheric aerosols is illustrated in Figure 6.13 which shows annual average fields derived from the AER model between 10 and 40 km altitude. Figure 6.13a shows the calculated mixing ratio of sulfate in aerosol particles, which peaks strongly in the tropics between 20 and 30 km. Stratospheric aerosol mass density in μg/m^3 is shown in Figure 6.13b, includes both sulfate and water. The number density of particles with radii greater than 0.01 μm is shown in Figure 6.13c. Highest particle densities are found in the tropical upper troposphere and near the tropopause. At high latitudes in the middle

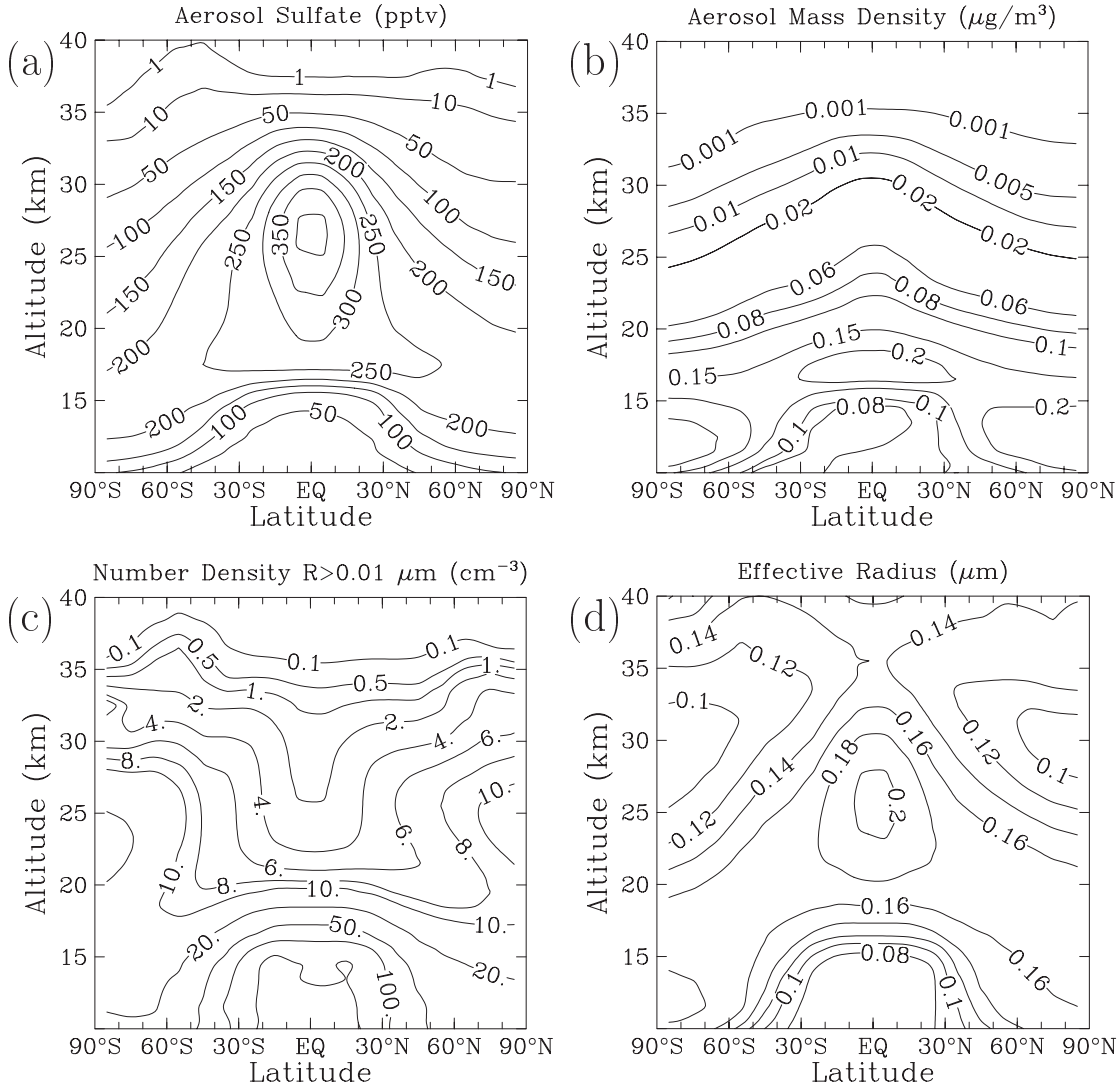

Figure 6.13: Model-calculated annual average morphology of the stratospheric aerosol layer showing (a) mixing ratio of sulfate in aerosol particles (pptv), (b) aerosol mass density (μg/m^3), (c) number density (cm^{-3}) for particles greater than 0.01 μm radius, and (d) effective radius (μm) from the AER model between 10 and 40 km.

stratosphere, nucleation takes place in winter and particle densities are greater than at low latitudes. Figure 6.13d shows the effective radius of aerosol particles, which maximizes in the tropical mid stratosphere and the high latitude lower stratosphere, indicating the most aged particles.

6.5.4 Comparisons to Satellite Extinction Measurements

Extinction observations from the SAGE II instrument provide the best spatial and temporal coverage of any stratospheric aerosol dataset. To make the comparisons between model simulations and observations as accurate as possible, Mie scattering codes are used to derive aerosol extinction from the model-calculated aerosol size distributions. Tropical and mid-latitudes profiles of model-calculated and SAGE background aerosol extinction at 0.525 μm are shown in Figure 6.14. More profiles can be found at http://www.sparc.sunysb.edu. The SAGE data shown are the two-year composite record of 2001 and 2002 representing a nonvolcanic background aerosol field as described in

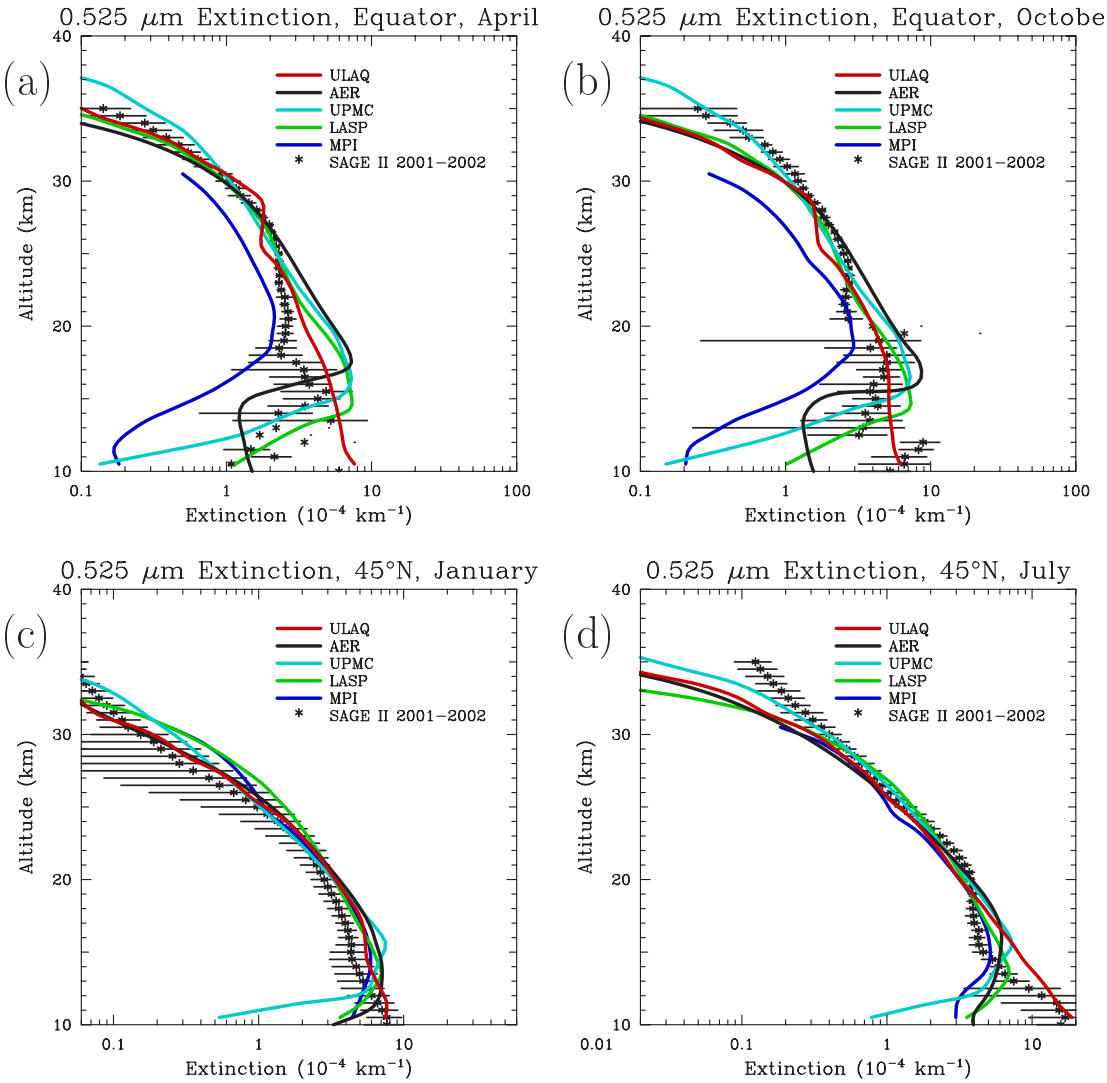

Figure 6.14: Comparison of SAGE II and model-calculated extinctions at 0.525 μm in (a) April and (b) October at the equator, (c) January and (d) July at 45°N. SAGE II data are a composite of 2001 and 2002 observations as described in the text.

Chapter 4, Section 4.2.1. Error bars on the SAGE II data are small relative to the plotted symbols between 20 and 30 km, but become larger outside this altitude range. On the log scale shown, the models generally agree with SAGE II observations above the tropopause at 45°N, though over predict somewhat from 12-18 km. At the equator, model results other than MPI match observations above 25 km, but the models often over predict below this altitude. Low extinctions in the MPI model in the tropics may be related to effects of the 30 km upper lid on the general circulation and overestimation of convective scavenging, along with a low value of SO_2 at the tropical tropopause. The observations show a sharp gradient in extinction at about 17 km in April or 20 km in October which the models are unable to reproduce. These gradients in the SAGE II data are unlikely to be due to clouds at the tropical tropopause, as clouds have been eliminated in these data through appropriate filters, though subvisible clouds cannot be fully excluded (see Chapter 4). The extinction in the 2-D models near the tropical tropopause is mainly a function of the imposed aerosol distribution there, whereas the 3-D models simulate the tropospheric sources and transport more accurately without imposed conditions at the tropopause. None of the models are able to reproduce the observed vertical gradients there. The observed aerosol extinction has more seasonal variability than the models. This could be an artifact of the lack of seasonal variability in the models' boundary conditions.

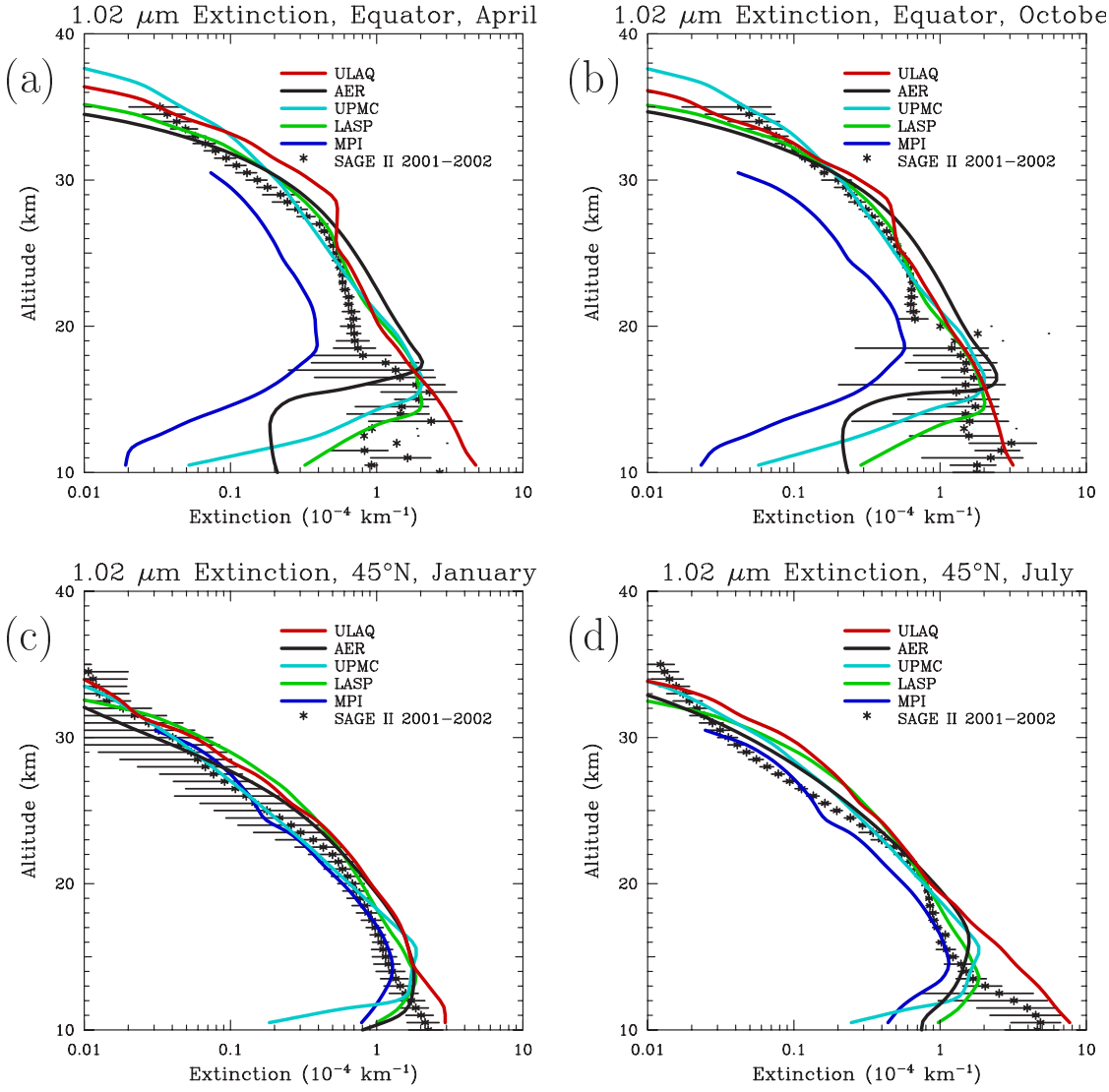

Figure 6.15: Comparison of SAGE II and model-calculated extinctions at 1.02 μm in (a) April and (b) October at the equator, (c) January and (d) July at 45°N. SAGE II data are a composite of 2001 and 2002 observations as described in the text.

Profiles of model-calculated and SAGE background aerosol extinction at 1.02 μm are shown in Figure 6.15. The models tend to overestimate the 1.02 μm extinction somewhat, though the UPMC and LASP models are generally within error bars between 25 and 35 km at the equator. All but the MPI model fall within error bars at the equator between 13 and 17 km in April and between 13 and 20 km in October. The UPMC and MPI models perform well at 45°N in January above 20 km and the other models are within or just above the error bars. In other months (see http://www.sparc.sunysb.edu) at 45°N, most of the models overpredict the 1.02 μm extinction at all altitudes, with ULAQ and LASP often higher than the other models. Model results at 45°S (see supplementary material) match observations better than at 45°N for April and October.

Model-calculated extinction profiles at 3.46 μm are shown in Figure 6.16 and compared with extinctions measured by HALOE averaged over the 1999-2004 period. Refractive indices at 3.46 and 5.26 μm are obtained from Tisdale et al. [1998]. Only the AER, UPMC, and MPI models provided 3.46 μm extinctions. AER and UPMC model results

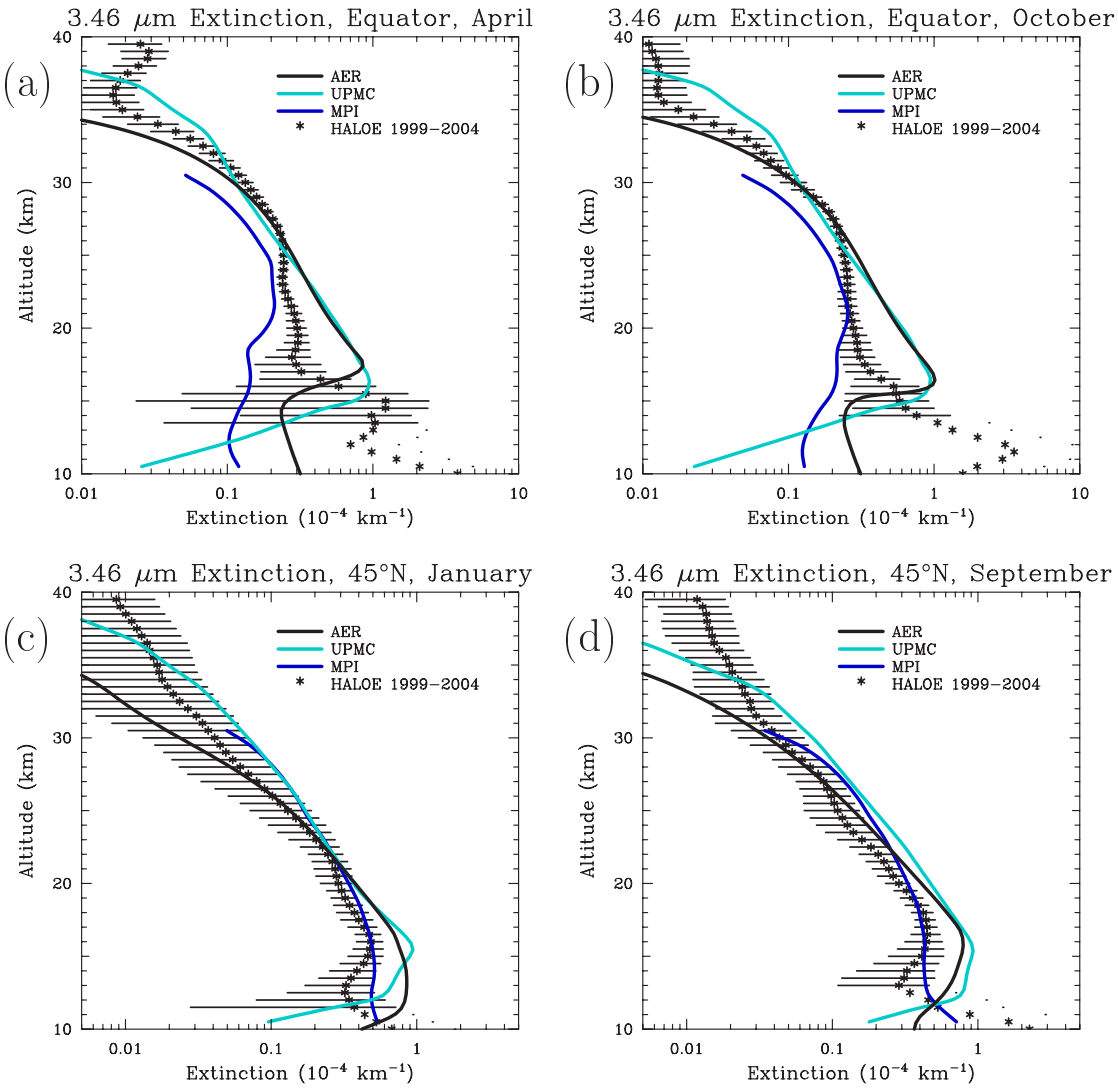

Figure 6.16: Comparison of HALOE and model-calculated extinctions at 3.46 μm in (a) April and (b) October at the equator, (c) January and (d) September at 45°N. HALOE observations are averaged over the 1999-2004 period.

are much higher than observations between 16 and 25 km in the tropics, while the MPI model consistently underpredicts in the tropics at almost all altitudes. The AER and UPMC models match observations between 26 and 30 km, but above 30 km the UPMC model is high and the AER model low. At 45°N the three models all fall within error bars in January above 22 km, but in September the UPMC model falls somewhat above error bars in this altitude range. All models except MPI overpredict below 22 km. Model-calculated extinction profiles at 5.26 μm are compared with HALOE observations in Figure 6.17. The model-calculated values tend to lie well below observations above 23 km in the tropics, though the UPMC model is close to the observations between 32 and 36 km. The ULAQ and UPMC models are near observations in the tropics below 23 km, while the AER model overpredicts there. At 45°N, the UPMC and MPI models are near observations, while the AER and ULAQ models show extinction that decreases too rapidly with altitude.

Overall, the models do a better job of reproducing the 0.525-μm extinction than the 1.02-μm extinction as measured by SAGE II. This may indicate that models have more difficulty reproducing the large end of the aerosol size distribution. Comparisons at 3.46

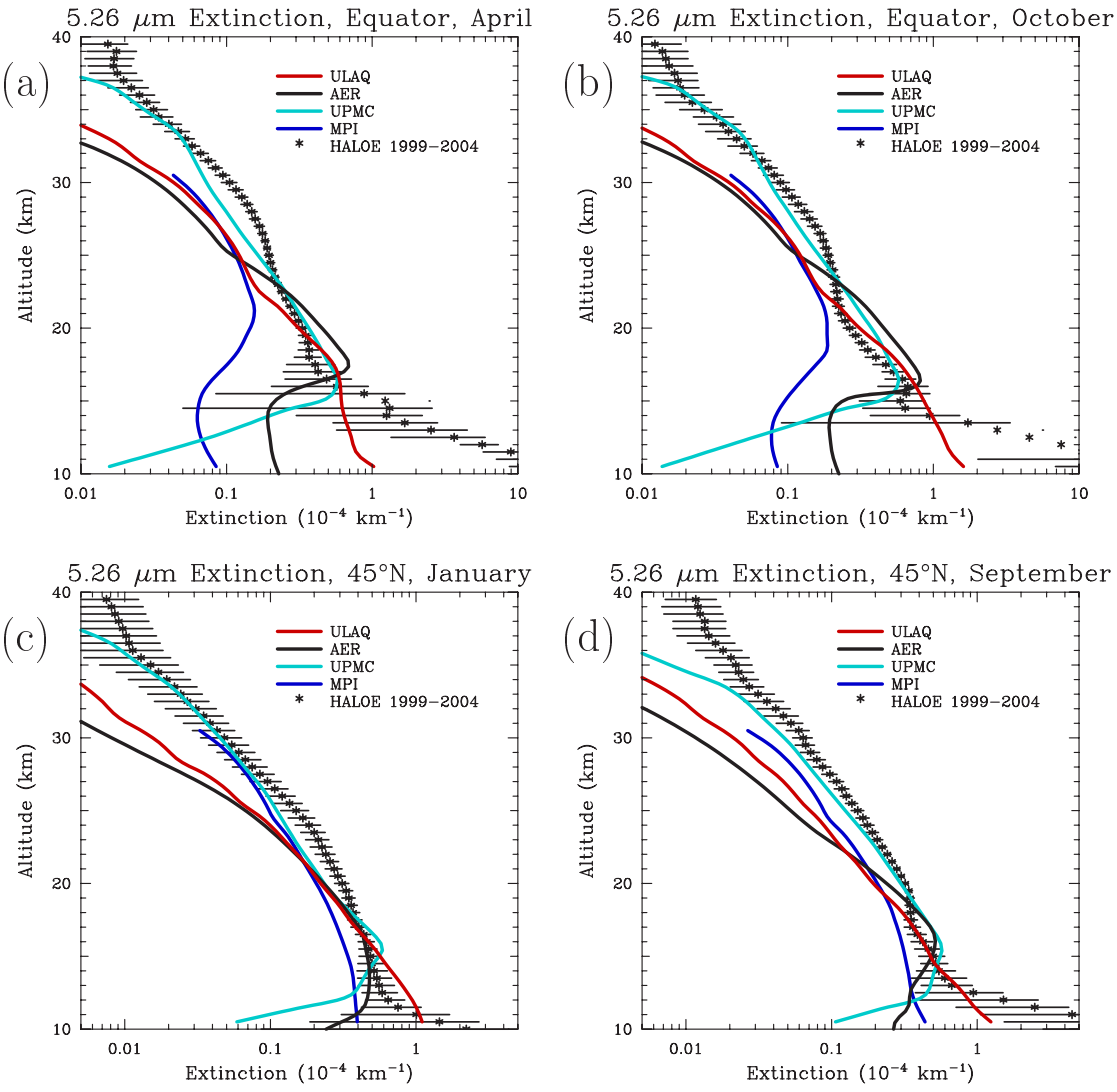

Figure 6.17: Comparison of HALOE and model-calculated extinctions at 5.26 μm in (a) April and (b) October at the equator, (c) January and (d) September at 45°N. HALOE observations are averaged over the 1999-2004 period.

and 5.26 μm show a larger spread among the models and significant differences with the HALOE observations. The tropical lower stratosphere proved difficult for any model to reproduce consistently due to strong vertical and seasonal gradients. If we assume that the high extinction values at and just below the tropical tropopause are due to sulfate aerosols, then the models cannot explain the much lower extinctions a few kilometers above the tropopause, since sulfate aerosols would not evaporate and sedimentation rates are small. The observations have been cleared of clouds, but could potentially be contaminated by subvisible cirrus, or could represent tropospheric aerosols, such as dust, soot from biomass burning, or particles with organic content which do not penetrate the stratosphere. There is indeed evidence that the fraction of sulfate in the aerosol directly below the tropical tropopause is just about 50%, dropping to less than 20% about 2-3 km lower [Murphy et al., 1998]. The models are essentially designed to simulate stratospheric aerosols, not tropospheric aerosols or clouds, and the influence of these aerosol types may be significant to the lowermost stratosphere. Additional years of SAGE data will improve the representativeness of this nonvolcanic observational dataset, which consists of only two years of observations in the current investigation.

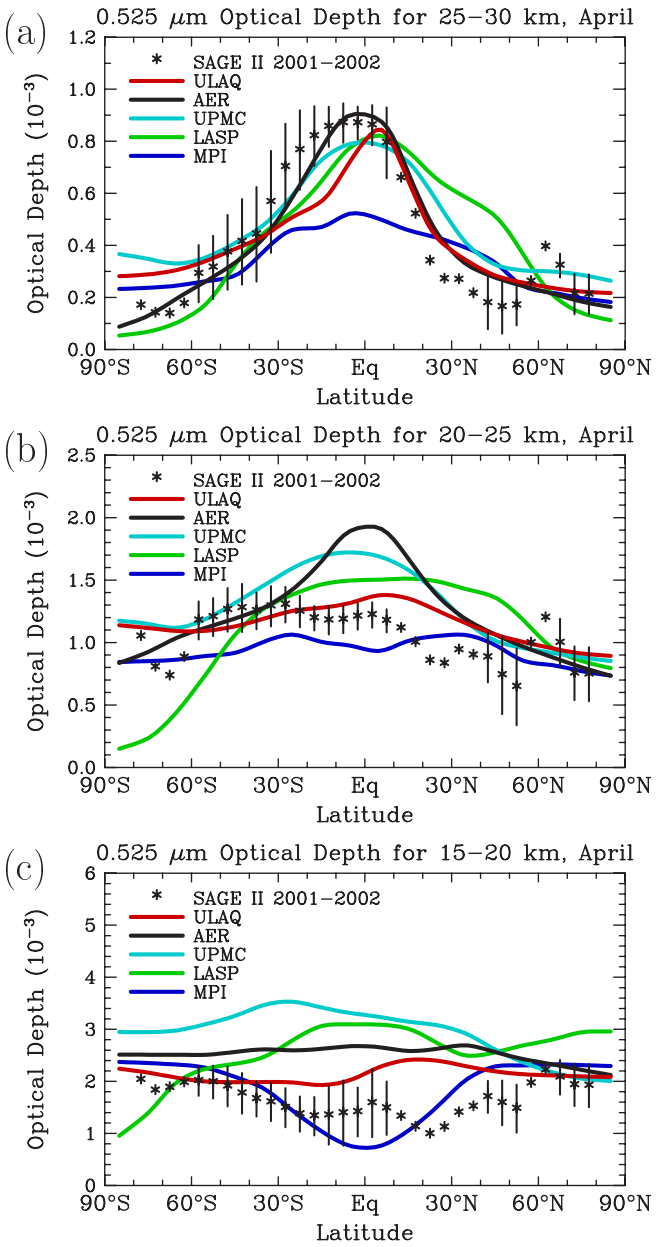

Figure 6.18: Aerosol optical depth at 0.525 μm for April of 2000 integrated from (a) 25 to 30 km, (b) 20 to 25 km and (c) 15 to 20 km. SAGE II data from the 2001-2002 composite background period are shown by symbols, model results by colored lines.

Aerosol optical depths at 0.525 μm as a function of latitude are shown in Figure 6.18 for April for the 15-20 km layer, the 20-25 km layer, and the 25-30 km layer. SAGE observations using the combined 2001-2002 nonvolcanic average are also indicated on the same plots. One should keep in mind that the lower part of the 15-20 km layer may be at or near the tropopause at tropical latitudes. SAGE observations show a strong latitudinal gradient in 0.525 μm optical depth in the 25-30 km layer, with equatorial

optical depths higher than mid and high latitude optical depths by factors of 2-4. The models generally reproduce this gradient and match the absolute value of optical depth well. In the 20-25 km layer, observational gradients are weak, but with high latitude optical depths generally lower than those at other latitudes. The models vary widely in this layer, with the AER model showing a strong peak in the tropics, the UPMC and LASP model showing weaker gradients which are also higher in low latitudes, and the ULAQ and MPI models showing little latitudinal gradient. The 15-20 km layer shows weak latitudinal gradients in the observations and most of the models, though several of the models predict optical depths that are too high by 50% or more. Similar plots for other months can be found in the supplementary material.

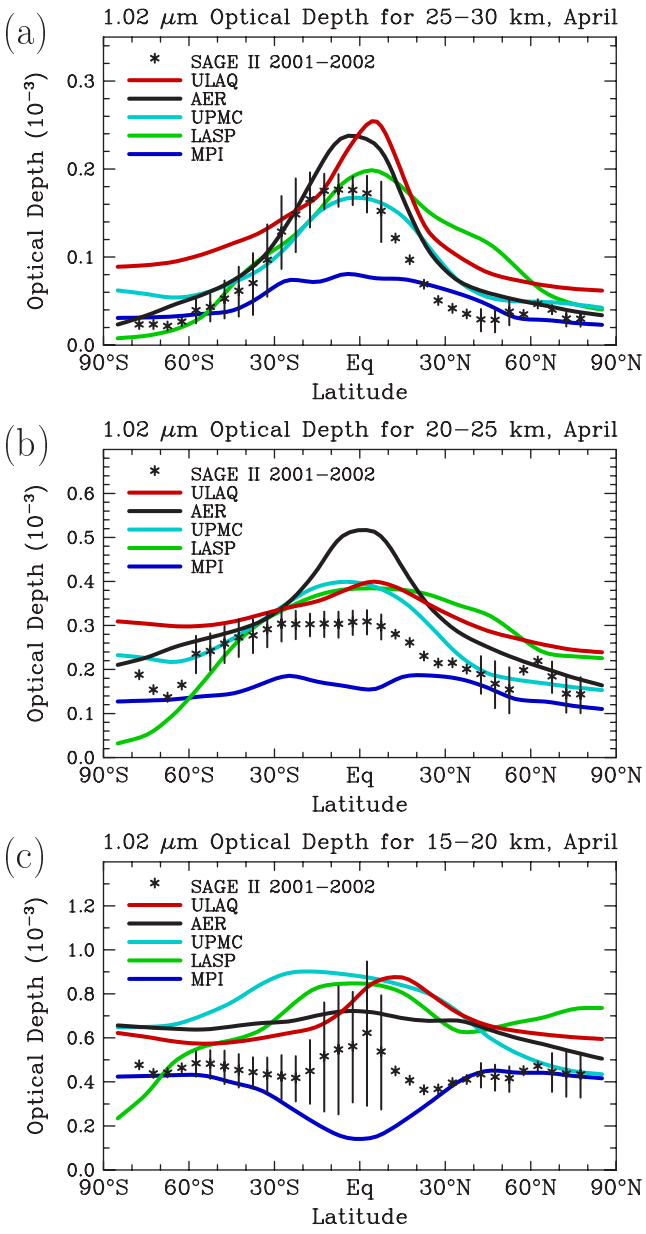

Figure 6.19: Aerosol optical depth at 1.02 μm for April of 2000 integrated from (a) 25 to 30 km, (b) 20 to 25 km and (c) 15 to 20 km. SAGE II data from the 2001-2002 composite background period are shown by symbols, model results by colored lines

Model-calculated and SAGE optical depths at 1.02 μm are shown in Figure 6.19. As found previously, the most pronounced differences between model simulations and SAGE observations are found in the 15-20 km region. Most models also overpredict the 1.02-μm optical depth in the 20-25 km region, but roughly approximate the latitudinal gradient there. In the 25-30 km region, models have significant spread, though the LASP, UPMC, and AER models match the magnitude of the observed optical depth over most of the southern hemisphere in April and much of both hemispheres in January (see supplementary material). The AER and ULAQ models are higher than observations in the tropics in April.

The comparisons between modeled and HALOE optical depths (Figures 6.20 and 6.21) show that most models underestimate optical depths at 5.26 μm in the upper and middle stratosphere regions, with the UPMC model performing better than the others. At 25-30 km, observations of 3.46 and 5.26 μm optical depth show an equatorial peak. At 5.26 μm, all models have too weak of a latitudinal gradient at this altitude, though the AER model matches the 3.46 μm optical depth quite well here. As with the SAGE wavelengths, observations show weak latitudinal gradients at 15-20 km and 20-25 km,

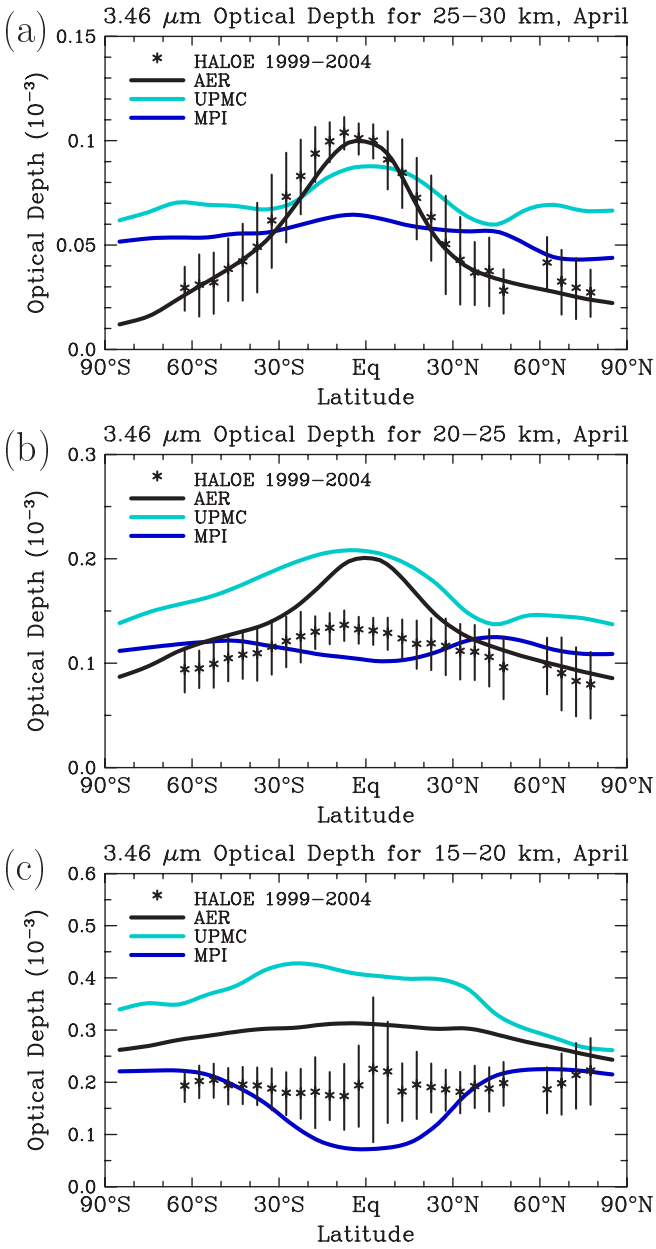

Figure 6.20: Aerosol optical depth at 3.46 μm for April of 2000 integrated from (a) 25 to 30 km, (b) 20 to 25 km and (c) 15 to 20 km. HALOE data averaged over the 1999-2004 period are shown by symbols, model results by colored lines.

but the models show a variety of latitudinal gradients in these altitude regions. Only the MPI model approximates the observed optical depths below 25 km at 3.46 μm, with the AER and UPMC models predicting optical depths too high.

These results are consistent with the previous comparisons of extinction profiles at selected latitudes. Since the models do not match observations at all compared wavelengths, it appears that the models do not accurately predict aerosol size distributions through the full range of particle sizes. The best comparisons are for the 0.525 μm wavelength, which is insensitive to particles less than ~ 0.1 μm radius. The 5.26 μm extinctions are sensitive to a broader range of particle sizes, and compare very poorly with observations above 25 km for most models. Reasons for this are not clear. Since the main loss process for larger particles is gravitational sedimentation in the middle stratosphere region, it is tempting to attribute the model bias to an inaccurate parameterization of this process in large-scale models. Another possible cause could be numerical diffusion caused by the limited aerosol size resolution used in global models. However, as shown in Section 6.6.1, this does not appear to be a major contributor to model differences with observed extinctions.

6.5.5 Comparisons to Derived Satellite Products

Up to this point, only the primary aerosol properties, extinction and optical depth (integrated extinction), measured by satellite instruments at different wavelengths have been used for the evaluation of the models (see Chapter 4). The equivalents to these primary measurements have been derived from the model-calculated aerosol size

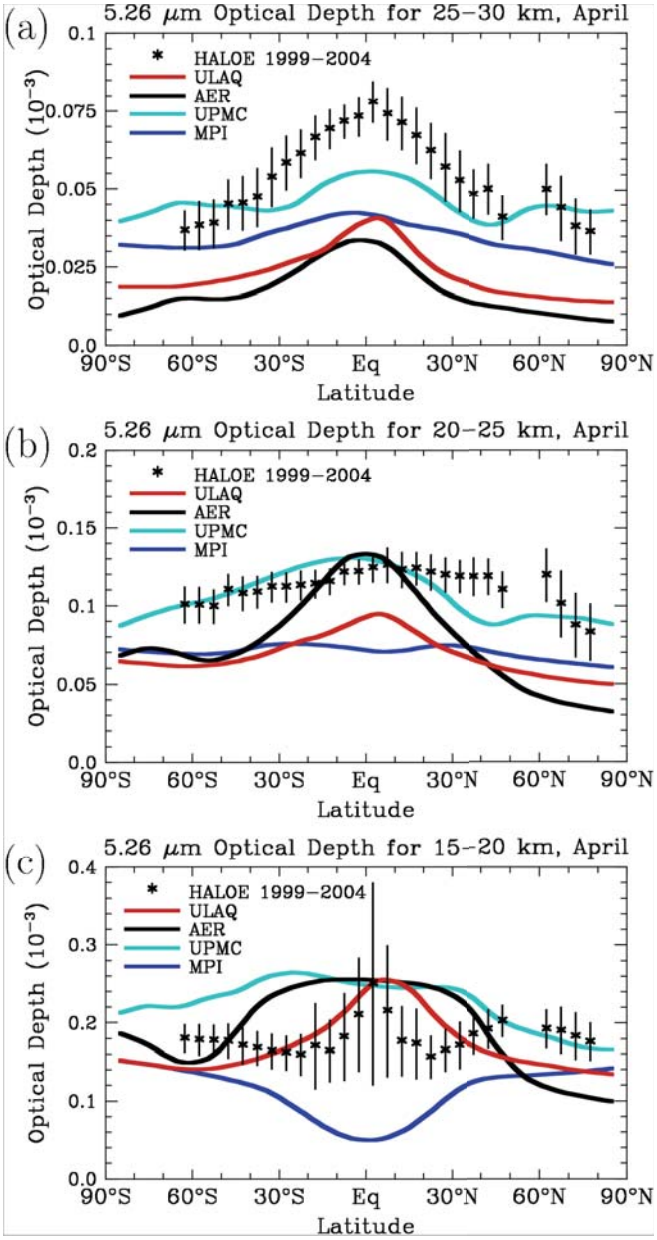

Figure 6.21: Aerosol optical depth at 5.26 μm for April of 2000 integrated from (a) 25 to 30 km, (b) 20 to 25 km and (c) 15 to 20 km. HALOE data averaged over the 1999-2004 period are shown by symbols, model results by colored lines.

distributions and Mie scattering codes. In this section, aerosol bulk properties (surface area density and effective radius) derived from SAGE primary multi-wavelength measurements are used for model evaluation and comparison. A description of the derivations and limitations of these satellite products is provided in Chapter 4, Section 4.2.1. The surface area densities and effective radii from the models are calculated using the entire size distribution available in the models. Surface area density profiles for two seasons at the equator and 45 °N are shown in Figure 6.22, with additional latitudes and seasons shown in the supplementary material. These results show greater inter-model variability than was seen for extinction. SAGE II values of surface area density are those derived from the 0.525 and 1.02 μm extinction using Equation 4.1 for the 2001-2002 composite year. The models tend to overestimate the surface area density relative to SAGE values, with the ULAQ model being the closest to SAGE surface area and the UPMC or LASP models being the highest. The most pronounced discrepancies between models and SAGE surface area are found in the lower tropical stratosphere. Only the ULAQ model comes close to SAGE results in this region. In comparison to SAGE surface area, modeled surface area appears to be overestimated by up to a factor 5-10 in some regions.

It is worth noting that while the comparisons with satellite extinctions apply Mie calculations to the modeled aerosol size distributions and therefore in principle capture the extinction of the full distribution for both models and measurements, this is not the case in the comparison with surface area density. In this case, the model result does again show a property of the full distribution, whereas the satellite instrument effectively underestimates the contributions from the smallest particles, and this effect is only partly corrected for by the retrieval algorithm (see Chapter 4). Therefore, the fact that the

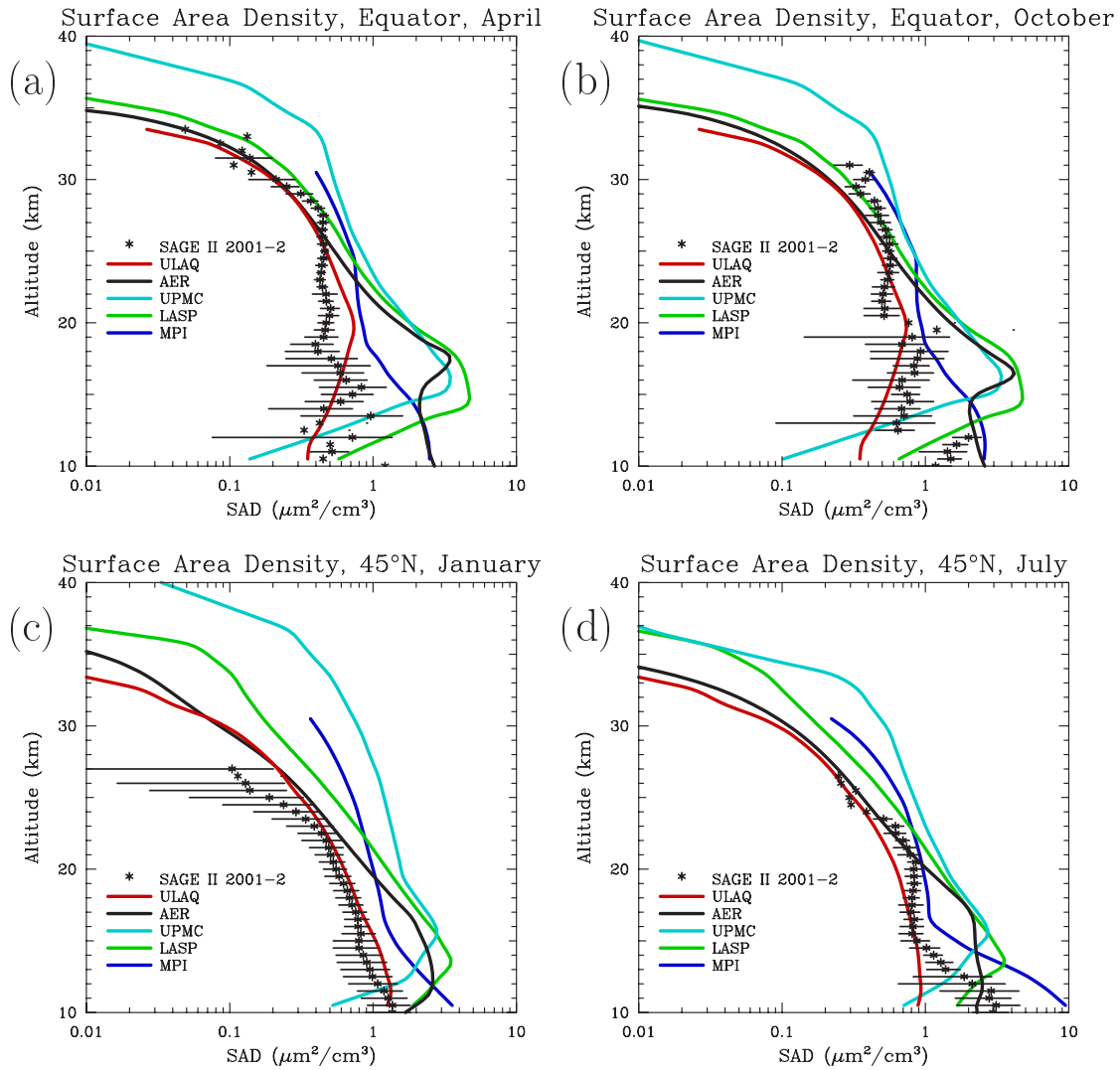

Figure 6.22: Comparison of SAGE II and model-calculated surface area density in (a) April and (b) October at the equator, (c) January and (d) July at 45°N. SAGE II results use Equation 4.1 to obtain surface area from the 2001-2002 composite of 1.02 and 0.525 μm extinction. Model-calculated surface area density is integrated over the model's entire size distribution

measured surface area densities are mostly smaller than the modeled ones is not surprising by itself. SAGE measurements are not very sensitive to particles smaller than 0.1 μm. As a result, the SAGE product underestimates the surface area in regions where the contribution of small particles is significant, such as the tropical tropopause region. This underestimation should be most apparent during background periods when the aerosol loading is low and the average size of the aerosol particles is the smallest.

In order to avoid the difference in particle size sensitivity between the satellite-derived surface area and the model-derived surface area, we have calculated surface area densities from the models using extinctions in the same manner as the SAGE II data product obtains surface area density (i.e. using the SAGE algorithm given in Equation 4.1). These extinction-derived surface area densities, shown in Figure 6.23, are considerably smaller than the corresponding integrated surface area densities for all models, except for the AER model above 25 km and the ULAQ model at some altitudes. Note that the ULAQ model is 3-D and includes tropospheric aerosol particles and more realistic tropospheric transport, which the 2-D models do not, but has the coarsest size resolution. The

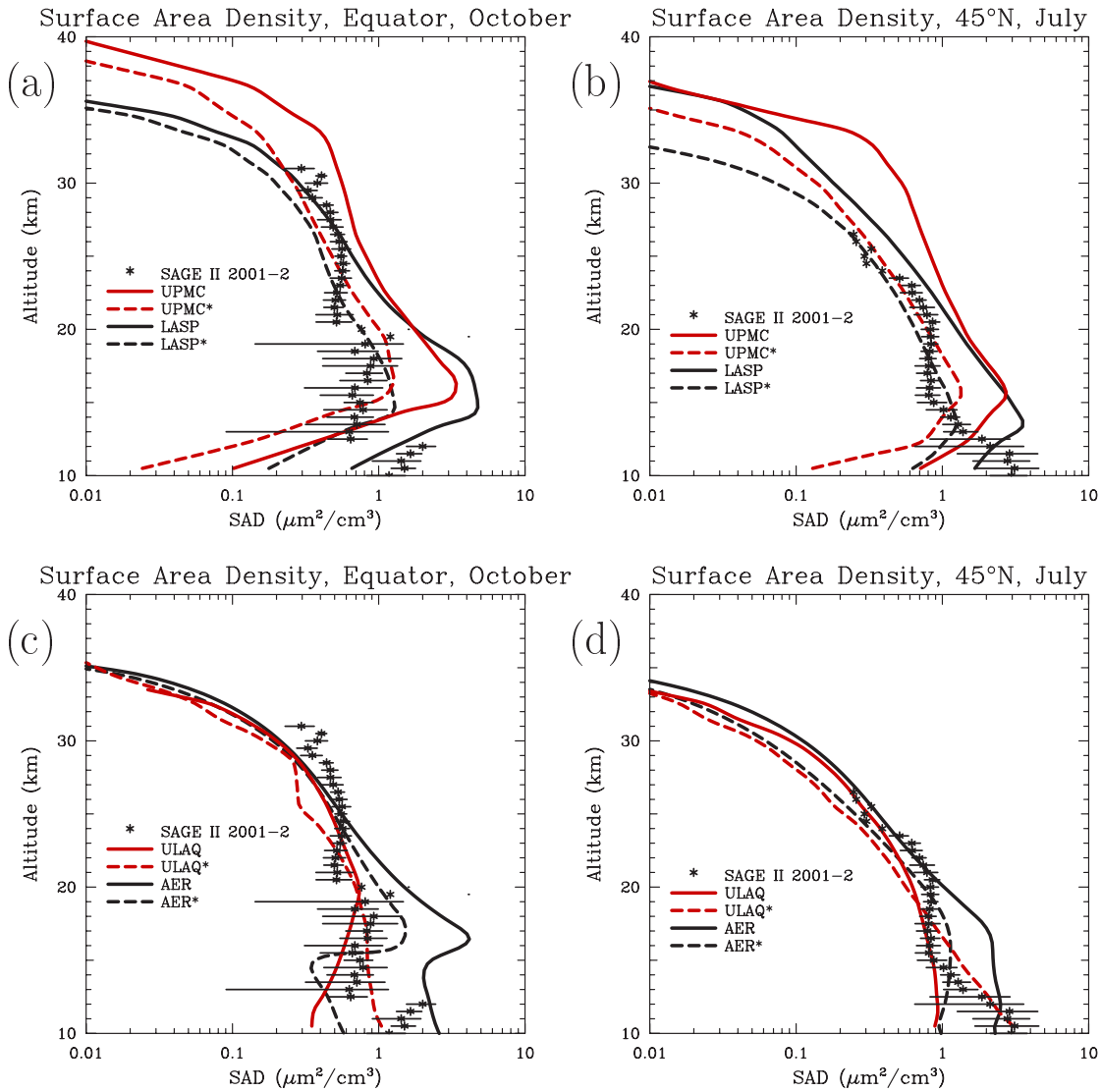

Figure 6.23: Comparison of surface area density derived from SAGE II observations (same as in Figure 6.22) and that calculated by the models at the equator in October (left panels) or 45°N in July (right panels). Dashed lines (labeled with a * after the model name) represent model surface area density derived from the 1.02 and 0.525 μm extinctions using Equation 4.1, while solid lines represent surface area density as integrated over the model's entire size distribution.

extinction-derived model results are often considerably closer to the SAGE-derived surface area densities.

We have calculated surface area density from the models employing lower limits on the particle size in the surface area integration. Figure 6.24 shows these results from the AER model, integrating over particles larger than 0.05 μm, particles larger than 0.1 μm, and particle larger than 0.15 μm. Integrals over particles greater than 0.05 or 0.1 μm differ from the full size distribution integration only below 25 km in the tropics or 20 km at midlatitudes, indicating that the particles smaller than 0.1 μm are only a significant contributor to the surface area density in the lower stratosphere. The integration over particles greater than 0.15 μm differs from the full integration at all altitudes. Integrating over particles larger than 0.1 μm yields a higher surface area than obtained by the extinction method, while integrating over particles larger than 0.15 μm yields a lower

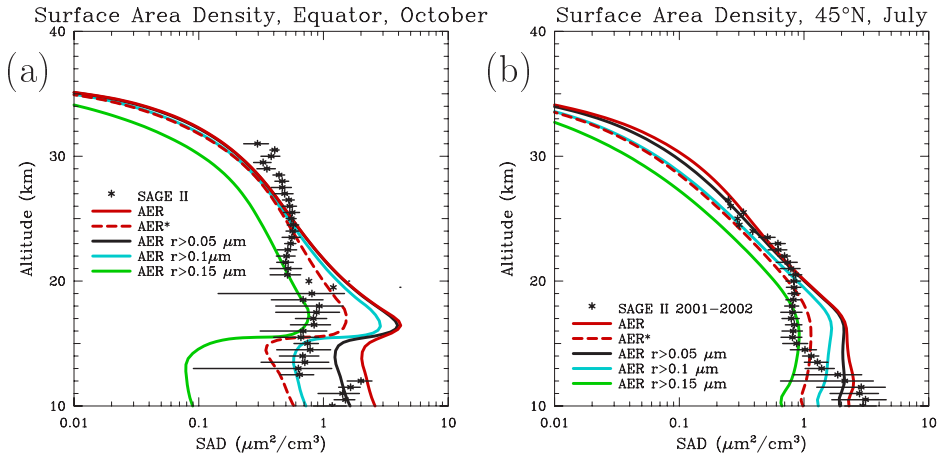

Figure 6.24: Comparison of surface area density derived from SAGE II observations (same as in Figure 6.22) and that calculated by the AER model at (a) the equator in October, and (b) 45°N in July. Dashed lines (AER*) represent model surface area density derived from the 1.02 and 0.525 μm extinctions using Equation 4.1, while solid lines represent surface area density as integrated over the model's aerosol size distribution with a lower radius cutoff as specified.

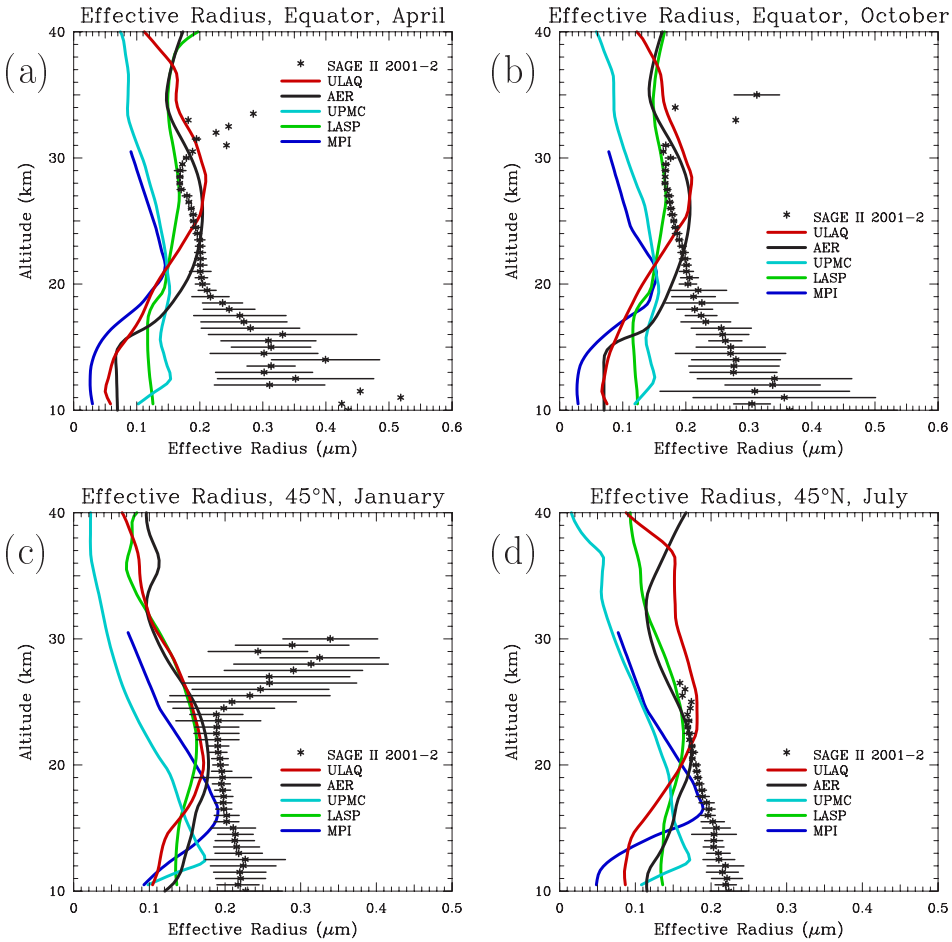

Figure 6.25: Comparison of SAGE II and model-calculated effective radius (a) April and (b) October at the equator, (c) January and (d) July at 45°N. SAGE II results use Equation 4.4 to obtain effective radius from the 2001-2002 composite of 1.02 μm extinction.

surface area which is within the range of SAGE II derived surface area density between 15 and 20 km but otherwise below it. Using a fixed size cutoff as we have done here is

not an accurate comparison with SAGE II derived surface area since extinctions show a range of sensitivity to aerosol particle size, not an abrupt cutoff. Yet it illustrates the inherent difficulty of comparing size distributions obtained from extinction measurements with model calculations. The lack of sensitivity of SAGE primary measurements to small particles probably explains much of the differences in the model-derived surface area density and the SAGE II derived surface area density. This explains why the differences between models and SAGE 0.525 μm extinction are very small compared to the differences in terms of surface area.

Aerosol effective radius is shown in Figure 6.25 for April and October at the equator and January and July at 45°N. SAGE II effective radius is derived from the 1.02 μm extinctions using Equation 4.4 for the 2001-2004 composite year. The models tend to produce lower effective radii than those inferred from the SAGE II instrument for the same reason that surface area densities tend to be higher, the lack of SAGE sensitivity to small particles. Models match SAGE II effective radii most closely between 20 and 30 km in the tropics, 15-25 km at 45°N, though the MPI and UPMC model generate smaller effective radii than SAGE II or the other models above 25 km. The model spread in effective radius ranges from 0.1 μm to 0.2 μm at 25 km at the equator, indicating that models differ substantially in the predicted size distributions.

6.6 Sensitivity Studies and Analyses

6.6.1 Sensitivity to model formulation

In this section we attempt to quantify the sensitivity of our results to the way in which the model represents the aerosol size distribution and to the formulation of some of the aerosol processes modeled. Where we can identify such differences, we can gain some understanding of the differences among the models used in this report. However, we make no attempt to diagnose intermodel differences or compare process formulations from model to model. Each model is a complex combination of many parameterizations and formulations and uses its own transport fields, so such an intercomparison is beyond the scope of this report. As a consequence, it cannot be shown here that models which use more precise representations of physical processes produce results more consistent with observations.

Sensitivity to bin resolution

Any aerosol formulation using fixed bin sizes suffers from numerical diffusion in size space, which may cause an increase in the width of the size distribution and may shift aerosol from small to larger bins too rapidly. The latter could result in excess sedimentation in the middle stratosphere and artificially lower the stratospheric aerosol burden. Global models, 3-D models in particular, must balance computational cost against accuracy. The AER 2-D model is capable of using a variety of aerosol bin resolutions, specified by the parameter V_{rat}, the volume ratio between consecutive bins, and the radius of the smallest bin R_{min}. We have made four sensitivity calculations using the AER model with different values of V_{rat} and R_{min} to test this sensitivity in a global model. Values of V_{rat} used include 1.2, 2.0, and 8.0. The AER, UPMC, LASP, and MPI models all employ V_{rat} values of 2.0. The ULAQ model uses a V_{rat} value of 8.0. Sensitivity studies used values of R_{min} of 0.39 nm and 10 nm at both V_{rat}=2.0 and V_{rat}=8.0. Of the models used in

this report, AER, LASP, and MPI use R_{min} values between 0.39 and 1 nm while the UPMC and ULAQ models use R_{min}=10 nm.

The calculations with different bin resolutions in the AER model show decreasing stratospheric aerosol mass density with increasing bin spacing (i.e. increasing V_{rat}). The effect on aerosol mass density of using V_{rat}=2.0 vs V_{rat}=1.2 is a few percent in the lower stratosphere at high latitudes, and up to 10% at 30 km. Using V_{rat}=8 relative to V_{rat}=2 leads to aerosol mass density decreases of 10-15% in the high latitude lower stratosphere and 25-30% at 30 km. Global stratospheric aerosol mass is lowered by ~ 10% in this case. Calculated size distributions are broadened with larger values of V_{rat}, producing more particles of both large and small size and fewer particles near 0.1 μm. Figure 6.26 shows profiles of aerosol extinction at 0.525 and 1.02 μm at the equator in October and 45°N in July from models with three different values of V_{rat}. The largest differences in extinction occur below the tropopause where nucleation occurs. Because the AER model considers only sulfate aerosols and has poor transport in the troposphere, the comparison with SAGE II data below the tropopause should not be used to validate the aerosol bin

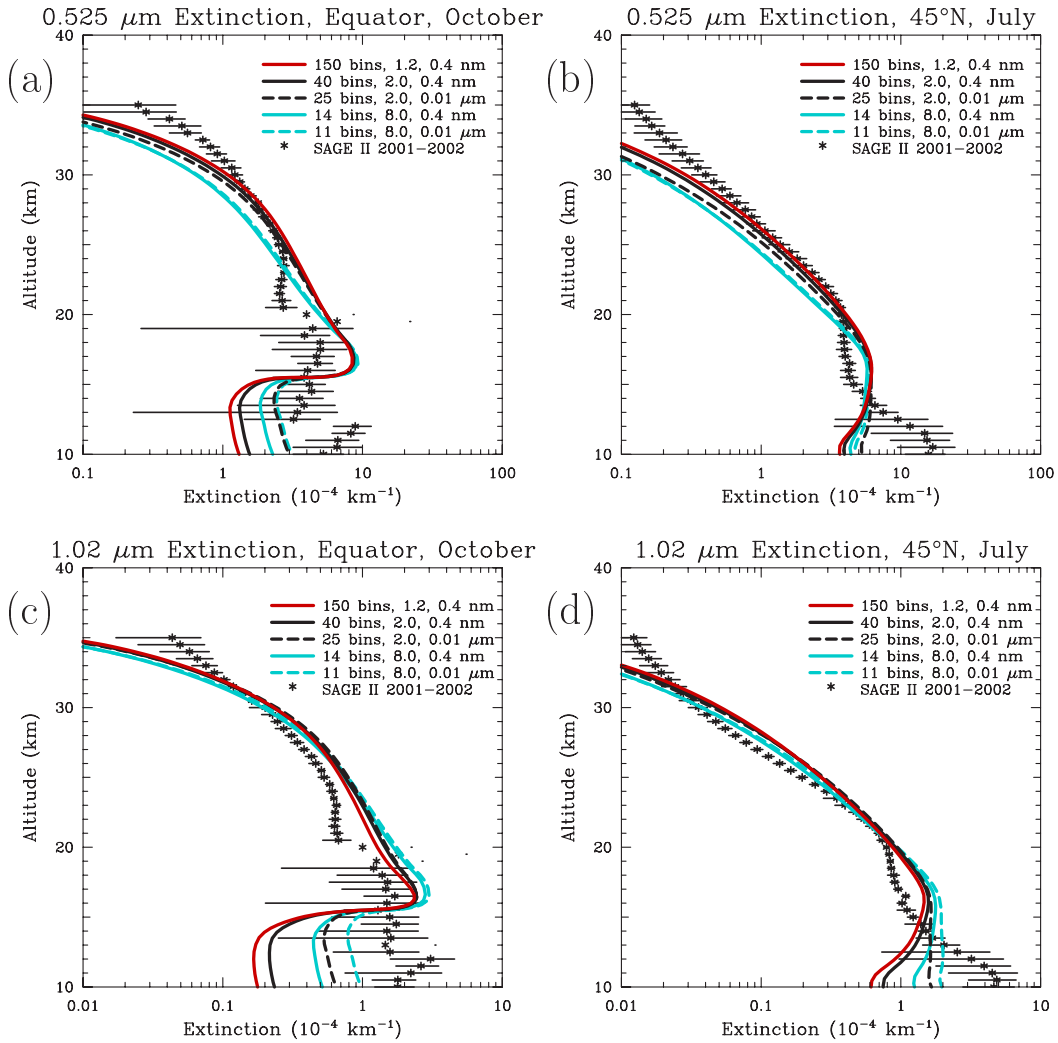

Figure 6.26: Comparison of SAGE II and calculated extinctions from the AER model at 1.02 μm at (a) the equator in October and (b) 45°N in July with different size resolutions. The numbers specified in the figure legend are number of size bins, volume ratio between adjacent bins (V_{rat}), and radius of smallest size bin (R_{min}).

resolution. Above the tropopause, larger values of V_{rat} lead to lower extinction values at 0.525 μm and higher extinction values at 1.02 μm.

The effect of increasing the smallest radius considered from 0.4 nm (the size of several molecules) to 10 nm changes the aerosol mass density only above 20-25 km, and modifies the global stratospheric aerosol mass by only 2%. Using a minimum radius of 10 nm forces the nucleated sulfuric acid mass into particles of this size, bypassing the coagulation process that would otherwise be required to achieve particles in this size range. This may in fact be preferable for global models, since their spatial resolution doesn't allow for localized nucleation, which would result in very high number densities and very high coagulation rates. The calculated size distributions are not greatly affected by the lack of small particles except in nucleation regions and evaporation regions. Figure 6.26 also shows the differences in extinction between models which are identical except for the value of R_{min} (compare solid and dashed lines of the same color). Below 15-18 km, the extinction is larger with larger R_{min}. Otherwise extinction differences due to R_{min} are small. Errors due to numerical diffusion caused by limited size resolution are found to be unlikely to explain most of the discrepancies between observed and modeled aerosol extinctions. Differences between models are not likely to be explained significantly by differences in bin resolution either, as other factors such as transport differences are probably more important.

Sensitivity to nucleation rate

Despite many years of experimental and theoretical research regarding nucleation of binary H_2O-H_2SO_4 aerosols, there is still an uncertainty of several orders of magnitude in nucleation rates of atmospheric aerosols [Hale et al., 2000]. While theories of classical binary homogeneous nucleation are well known, calculations from these theories do not always match observations. These theories have been modified by considering hydrated sulfate clusters and ternary nucleation involving ammonia [Kulmala et al., 2000] or nucleation on organics [O'Dowd et al., 2002] or chemiions [Yu and Turco, 2000; Lovejoy et al., 2004]. In addition, nucleation likely occurs in the atmosphere in the vicinity of deep convective events and where gravity waves induce temperature fluctuation, situations not spatially resolved in global models. Nucleation processes are discussed in Chapter 1, Section 1.5.1 of this report. Here we investigate the sensitivity of our model results to a standard nucleation parameterization and to the thermodynamic upper limit of nucleation. The upper limit is obtained by assuming that the collision of any two sulfur molecules at their thermal speed results in a new particle, with the appropriate water fraction condensing instantaneously.

The AER model was run with the Vehkamäki et al. [2002] nucleation scheme and the thermodynamic upper limit. Total atmospheric nucleation was larger by over two orders of magnitude when using the upper limit. This results in more particles of smaller mean size. Surface area density increases by up to 80% in the tropical upper troposphere with increased nucleation, but only by 5-20% in most of the stratosphere. Aerosol mass density does not change below 20 km, but increases by 5-15% above 20 km and up to 30% at 30 km. This indicates the lessening of the effect of gravitational settling on the slightly smaller particles, once they have sufficiently long travel times in the middle stratosphere. Global aerosol mass remains almost unchanged. Changes in stratospheric aerosol extinction are small (less than 10% at 1.02 μm). Coagulation acts as a self-limiting

process to limit the sensitivity of stratospheric aerosol to nucleation, which occurs mostly in the upper tropical troposphere.

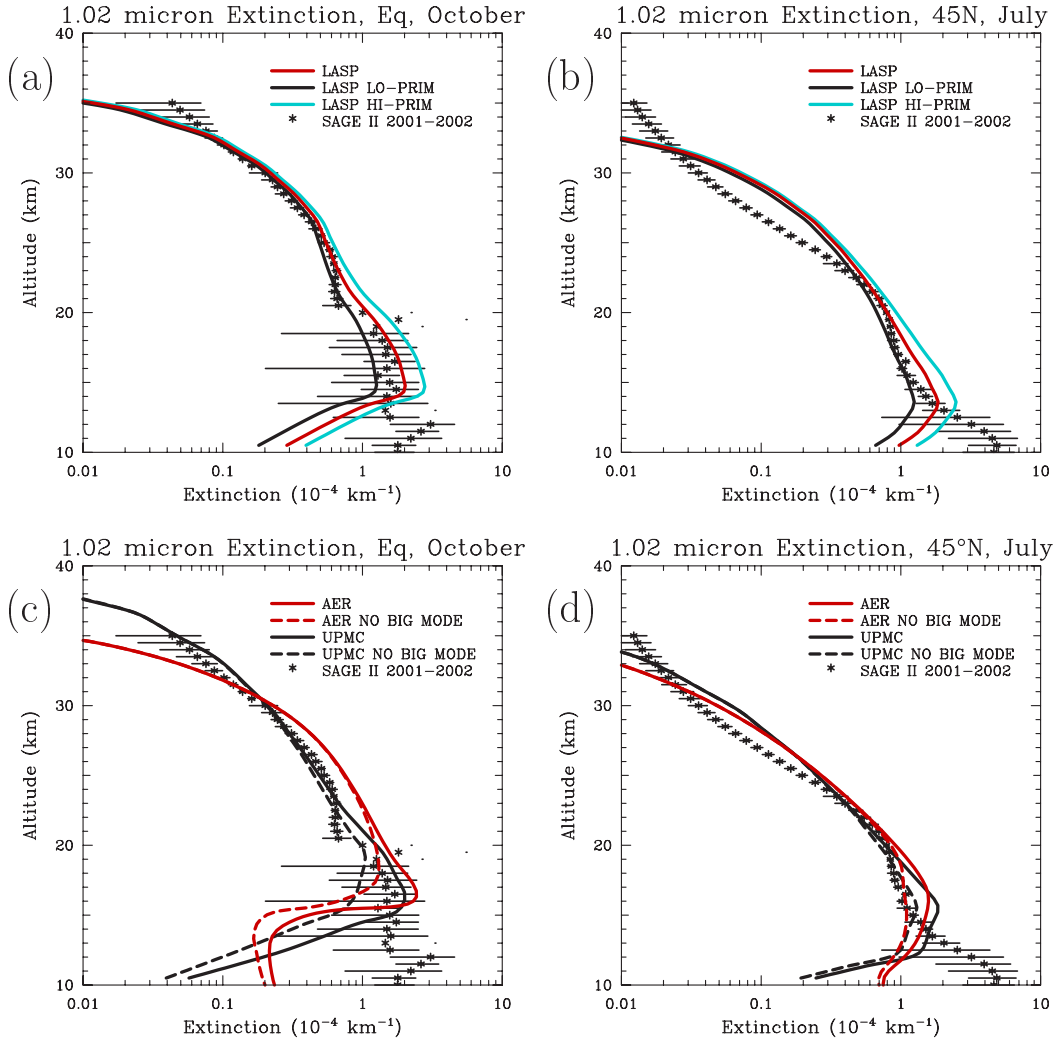

Figure 6.27: Comparison of SAGE II and model-calculated extinctions at 1.02 μm in October at the equator (left panels) and 45°N in July (right panels) from the LASP, AER, and UPMC 2-D models using different tropopause boundary conditions for primary primary aerosol. LO-PRIM has primary aerosol concentration reduced by two standard deviations (to 160 pptv), HI-PRIM has primary aerosol concentration increased by two standard deviation (to 356 pptv), and NO BIG MODE has removed the particles greater than 0.3 μm from the primary aerosol distribution.

6.6.2 Primary aerosol sensitivity

While the ULAQ 3-D model used in this report has its own tropospheric aerosol scheme, the 2-D models (LASP, AER, and UPMC) need to prescribe the amount of condensible material and aerosol at the tropical tropopause. To test the sensitivity of our results to the assumed aerosol concentration and size distribution at the tropical tropopause, we have performed sensitivity studies with the LASP, AER, and UPMC models. These sensitivity studies provide not only model sensitivity to this parameter, but an indication of the importance of particles transported across the tropical tropopause to the stratospheric aerosol budget.

The LASP model performed calculations to vary the tropopause aerosol input concentration over the two standard deviation (37%) range reported by S.-H. Lee (Figure 6.9) while maintaining the same size distribution. Figures 6.27a and 6.27b show profiles of 1.02 μm extinction from the LASP model at the equator in October and at 45°N in July. Additional months, as well as 0.525 μm extinctions, are shown in the supplementary material. Aerosol extinctions above 25 km are insensitive to aerosol crossing the tropopause, being primarily related to sulfur derived from OCS. Results labeled "LO-PRIM" used 160 pptv of tropopause primary aerosol and results labeled "HI-PRIM" used 356 pptv of tropopause primary aerosol. The standard tropopause aerosol produces the best fit to observations at the equator in October in the 14-20 km region in the LASP model, with results from model calculations with tropopause aerosol reduced or enhanced by two standard deviation also within the error bars of the SAGE II observations. At 45°N in July, the LASP model results at the lower limit of tropopause aerosol fit the observations better between 14 and 20 km.

Figures 6.27c and 6.27d show profiles of 1.02 μm extinction from the AER and UPMC models with the larger mode (0.3-0.8 μm radius) of the primary aerosol eliminated. This decreases the input sulfur mass at the tropical tropopause by 25%. If the large aerosol mode reported by S.-H. Lee were not pure sulfate, but rather tropospheric particles of a different composition, or solid particles coated with sulfate, then those particles would contribute to the extinction near the tropopause but not to the sulfur burden of the stratosphere. The large primary aerosol mode has a big effect on extinction between 15 and 20 km in the tropics and a more modest affect at 45°N. Comparisons with observations in the tropics show that results with and without the large mode of primary aerosols are all within the observational error bars in the tropics below 18 km, though results without the large mode are a better fit between 18 and 22 km. At 45°N in July, model results without the large mode are a better match to observations. Aerosol mass is unchanged above 20 km with or without the large mode primary particles, confirming that these particles do not penetrate into the middle stratosphere in our model simulations.

Shown in Figure 6.12, the AER model's sulfur budget changes with tropopause aerosol input. The primary aerosol input to the stratosphere varies from 50 to 82 kilotons of sulfur per year over the one sigma range discussed here. This results in a range of the stratospheric aerosol burden from 170 to 204 kilotons of sulfur. The change in primary aerosol of ±19% (one sigma range) leads to an aerosol mass mixing ratio change of -8 to +10%. In the case with the large particles removed from the primary aerosol distribution, the influx of primary aerosol to the stratosphere is 43 kilotons of sulfur per year and the stratospheric burden 174 kilotons of sulfur.

6.6.3 Tropopause SO_2 sensitivity

The AER and LASP models performed sensitivity studies to the imposed SO_2 concentration at the tropopause. The standard simulation used 40 pptv of SO_2 and 258 pptv of primary aerosol at the tropopause. Measured SO_2 concentrations in the upper troposphere vary widely, up to 200 pptv [Thornton et al., 1999], and we have chosen upper and lower limits of 0 and 80 pptv of tropopause SO_2 for our sensitivity tests. The SO_2 concentrations near the tropopause do not have an immediate direct effect on local aerosol because reaction with OH and then gas-to-particle transformation are required. Changes in tropopause SO_2 concentration will lead to changes in aerosol number through nucleation, and will affect particle size through condensation. We find the sensitivity of

extinction at 1.02 or 0.525 μm to tropopause SO_2 to be quite small when primary aerosol is included in the simulations from both the AER and LASP models. This is because the SO_2 range tested (±40 pptv) is small compared to the imposed primary aerosol sulfur concentration (258 pptv) and because the impact of additional SO_2 on the large particle sizes which scatter visible light is small.

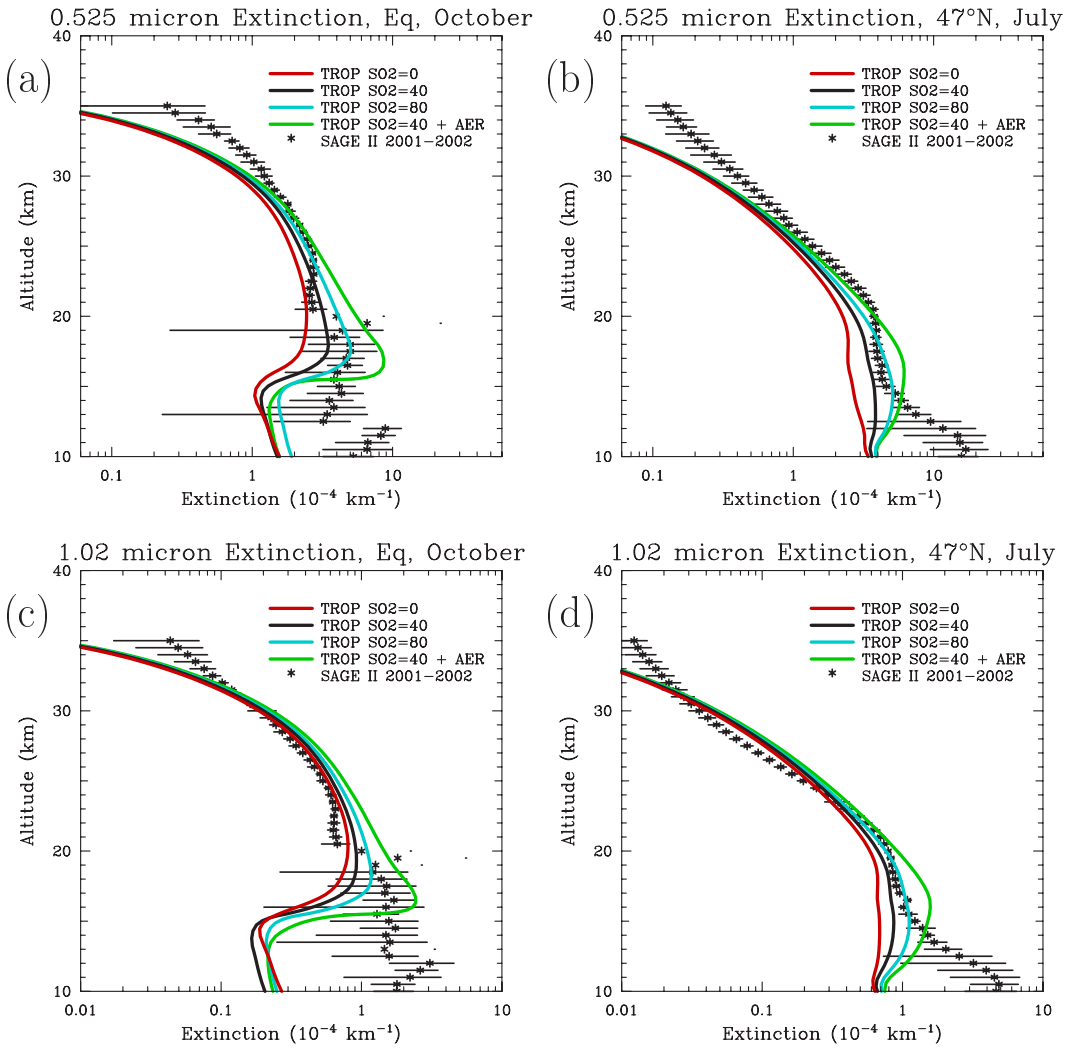

Figure 6.28: Comparison of SAGE II and model-calculated extinctions at 0.525 μm (top panels) and 1.02 μm (bottom panels) in October at the equator (left panels) and 45°N in July (right panels) from the AER 2-D model using different tropopause boundary conditions for SO_2 (0, 40, and 80 pptv) without primary aerosol and for SO_2 of 40 pptv with primary aerosol.

The AER model was used for simulations without primary aerosol but with tropopause SO_2 of 0, 40, and 80 pptv. Extinctions at 0.525 and 1.02 μm are shown in Figure 6.28 for these simulations. A calculation with primary aerosol and 40 pptv of tropopause SO_2 is also shown for comparison. There is strong sensitivity of extinction to tropopause SO_2 over the range modeled, with the 0.525 μm extinction showing more sensitivity than the 1.02 μm extinction. Tropopause SO_2 impacts stratospheric aerosol extinction as high as 30 km, at greater altitudes than those showing sensitivity to tropopause primary aerosol in the AER model. In the 15-25 km altitude range, the simulation with no primary aerosol and tropopause SO_2 of 80 pptv produces less extinction than with the lower limit (160 pptv) of primary aerosol. In the tropics in October, the simulation with 80 pptv of

SO_2 matches SAGE II 0.525 μm observations between 15 and 20 km. At the same time and latitude, the 1.02 μm SAGE II extinction between 20 and 30 km is matched best by the simulation with no tropopause SO_2. Among the simulations with modified primary aerosol and tropopause SO_2 amounts, none are a universally good match for SAGE II observations from 1999-2000. The vertical and latitudinal variations observed in SAGE II extinctions are not reproduced well by the models.

6.6.4 OCS sensitivity

Observations of OCS mixing ratios discussed in Chapter 2 indicate considerable variability on seasonal time scales and as functions of latitude, longitude, and altitude. Observations at the Jungfraujoch, Lauder, and Wollongong indicate long-term trends of -5%/decade, -6.9%/decade, and -3.5%/decade (see Section 2.3.1 for details). These trends, while small but statistically significant, may have had implications for stratospheric aerosol levels. We have investigated the sensitivity of model-calculated aerosol loading to changes in tropospheric OCS by decreasing the surface mixing ratio of OCS by 10% in the AER model. This results in a decrease of only 3% in the global stratospheric aerosol mass burden, and local decreases in mass density and surface area density of up to 6% and 5%, respectively above 25 km. As discussed in Section 6.5.3, OCS forms the primary aerosol source above 25 km, while SO_2 and particles transported from the troposphere are more important below. Extinctions at 0.525 and 1.02 μm decrease by 7% and 9%, respectively, above 20-25 km when OCS is reduced by 10%.

6.7 Model Simulations of Volcanic Conditions

6.7.1 Description of Calculations

The models have performed a simulation of the evolution of the stratospheric aerosol following the Mt. Pinatubo volcanic eruption in the Philippines on June 15, 1991. Models were initialized with 20 megatons of SO_2 [Bluth et al., 1992; McCormick et al., 1995] in the 16-30 km altitude region [Read et al., 1993] over the tropical site. Each model makes somewhat different assumptions concerning the vertical and horizontal distribution of the volcanic SO_2, with the ULAQ model injecting no SO_2 below 21 km. Subsequently the SO_2 is converted to H_2SO_4 via reaction with OH. OH fields are either calculated or prescribed in the models, yielding an e-folding time for SO_2 chemical loss of approximately 30 day. Nucleation rates are enhanced over background conditions for the first few months following the eruption. However, the majority of the volcanic sulfur is converted to aerosol by condensation onto preexisting particles, resulting in larger stratospheric aerosol particle sizes for several years. In agreement with observations, the models calculate that the perturbation decays with e-folding times of about 1 year, with near-background levels reached again in the late 1990s.

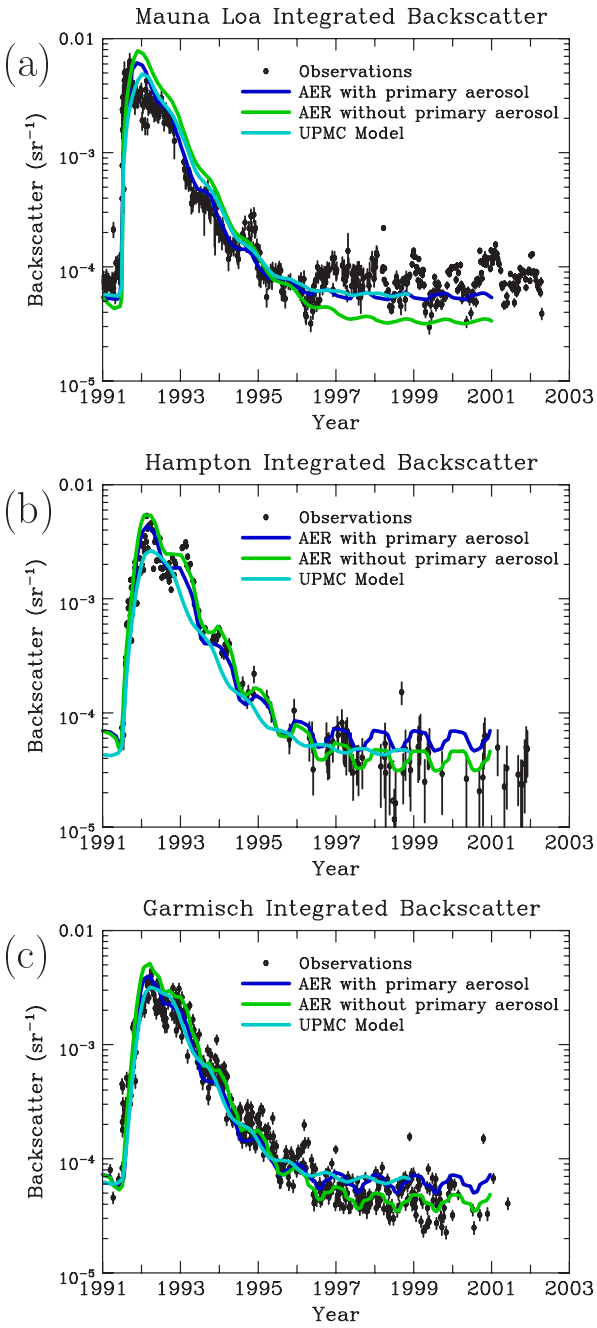

Figure 6.29: Integrated lidar backscatter at 694 nm at (a) Mauna Loa (19°N, 15.8-33 km) (b) Hampton, VA, (37°N, tropopause to 30 km) and (c) Garmisch-Partenkirchen (47°N, tropopause + 1 km to top) for the post-Pinatubo period. Observations are shown by black dots with error bars, model results by solid lines. AER model results are shown both with and without assumed primary aerosol entering the stratosphere at the tropical tropopause.

6.7.2 Comparisons with Lidar Backscatter Measurements

The evolution of Mt. Pinatubo volcanic aerosols has been monitored at several lidar measurement stations. Model-calculated backscatter columns (i.e. backscatter integrated vertically) are compared to observations at a tropical site (Mauna Loa at 19°N) and two midlatitude sites (Hampton at 37°N and Garmisch-Partenkirchen at 47°N) in Figure 6.29. The lidar instruments, which operate at about 0.67 μm, are discussed in Chapter 3, Section 3.3.2, and the lidar data in Chapter 4, Section 4.1.3. Column integrals at Mauna Loa include 15.8 to 33 km, at Hampton from the tropopause to 30 km, and at Garmisch from 1 km above the tropopause to the top of the aerosol layer. The evolution of the backscatter column can be decomposed into three phases: a very steep increase, a maximum, and a slow decay toward background levels. The steep increase in backscatter column is reproduced by the models (AER, UPMC). The lidar data show that the backscatter column peaks earlier at Mauna Loa (about 3-6 months) compared to the midlatitude sites (8 or 9 months); this is also the case in the models but the difference between the sites is not as pronounced. The magnitude and timing of the maximum observed at midlatitude stations is reproduced by the models. However, the maximum at Mauna Loa occurs later in the models.

Overall, the model-calculated values appear to match rather well the lidar measurements during the slow decay toward background values. Mauna Loa observations may reflect the volcanic eruption of Rabaul on September 14, 1994 which the models did not simulate. AER model results with and without prescribed primary aerosol entering the stratosphere at the tropical tropopause are shown, the difference being small except after 1996. The simulation with

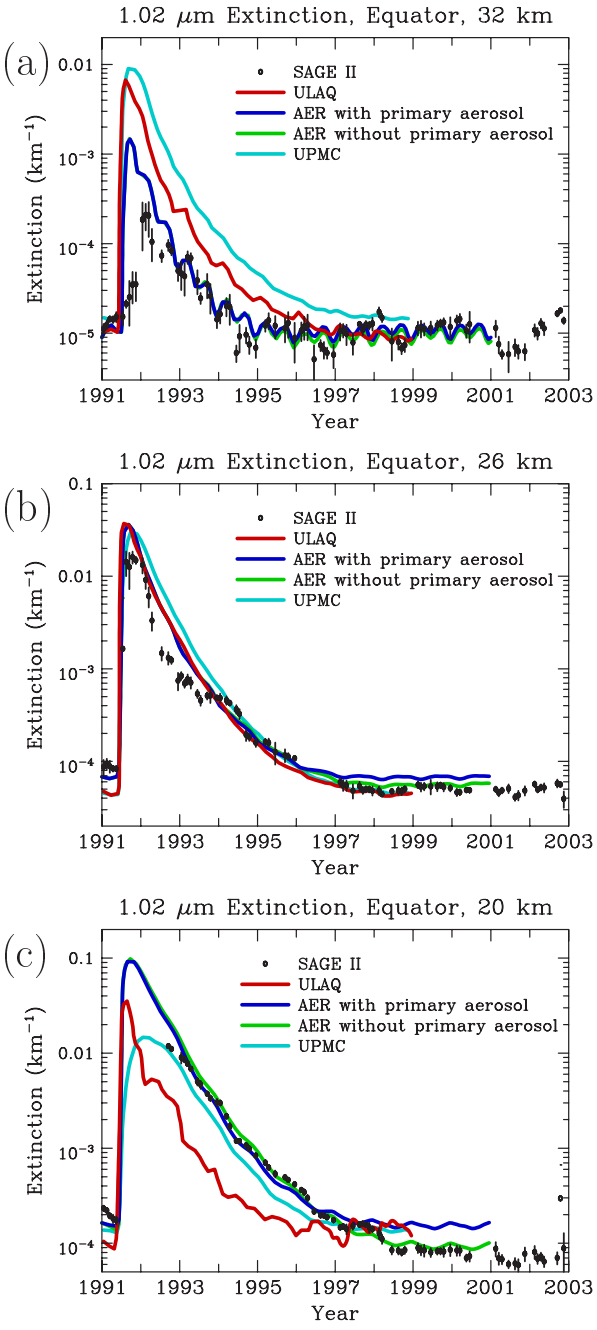

Figure 6.30: Aerosol extinction at 1.02 µm for 1991 to 2002 at the (a) equator and 32 km, (b) equator and 26 km, and (c) equator and 20 km. SAGE II data are shown by black symbols with error bars, model results by colored lines.

primary aerosol appears to match the Mauna Loa observations best, while the simulation without primary aerosol matches best at Hampton. The variability in the Garmisch data is as large as the difference in the two AER simulations. The pronounced annual cycle in the model calculated integrated backscatter at midlatitudes is due mostly to the shifting tropopause height. As expected, the lidar data exhibit much more variability than the model simulations which represent a zonal average. The observations show variability on short-term and inter-annual timescales. This variability is of dynamical origin and is vastly underestimated in the models. The variability makes it difficult to define exactly background aerosol levels in the lidar data. As a result, the timing of the return to a background state can only be defined as a return to within this background variability. The higher the background variability of an aerosol parameter is compared to the volcanic perturbation, the quicker the return to the background level appears to be. For example, the variability in the measured backscatter column at Mauna Loa is very high, giving the impression that the return to background levels occurred in 1995, several years earlier than at midlatitude sites. In contrast, there is little variability in the model-calculated integrated backscatter. Consequently, the background backscatter level is relatively well defined. The models predict a return of the backscatter column to the background level not before 1997.

Lidars are not sensitive to small aerosol particles. Therefore, the backscatter column is mainly a measure of medium to large aerosol particles (typically particles greater than a tenth of a micron). As most of the aerosol mass is contained in this size range, the backscatter also provides an estimate of the aerosol mass loading. The ability of the models to reproduce the broad features of the evolution of the backscatter column indicates that the evolution of the aerosol mass loading is adequately simulated in the

models, with an overall sufficiently accurate description of particle nucleation, growth, coagulation, evaporation, sedimentation, and dynamical transport.

6.7.3 Comparisons with SAGE II Observations

The evolution of 1.02 μm extinction at the equator (Figure 6.30) over the 1991 to 2002 period shows that the aerosol extinction starts increasing immediately after the Pinatubo eruption. The model-simulated extinctions increase at approximately the correct rate at 26 km, but much too rapidly at 32 km, with model simulations of 32 km extinction rising almost as rapidly as the 26 km extinction. There were no SAGE II data available at 20 km shortly after the eruption because of the large optical thickness of the aerosol cloud. At 26 km, all three models (ULAQ, AER, UPMC) do a reasonable job at simulating the 1.02 μm extinction over the entire period except in 1992 and 1993, when model calculations are too high compared to SAGE observations. At 20 km, the AER and UPMC models match the SAGE II extinctions fairly well, while the ULAQ modeled values are too low. AER model simulations both with and without imposed primary aerosols at the tropical tropopause are shown; they differ at 20 km in the tropics, but not significantly at the other altitudes. The AER simulation without primary aerosol drops to lower levels after 1997, matching better the SAGE 20 km extinctions. At 32 km, the AER model simulations are close to the observations after 1992, while ULAQ and UPMC modeled values are too high. This would indicate that either the upward transport in the ULAQ and UPMC models is too strong in the tropics or that the volcanic SO_2 cloud was placed too high initially.

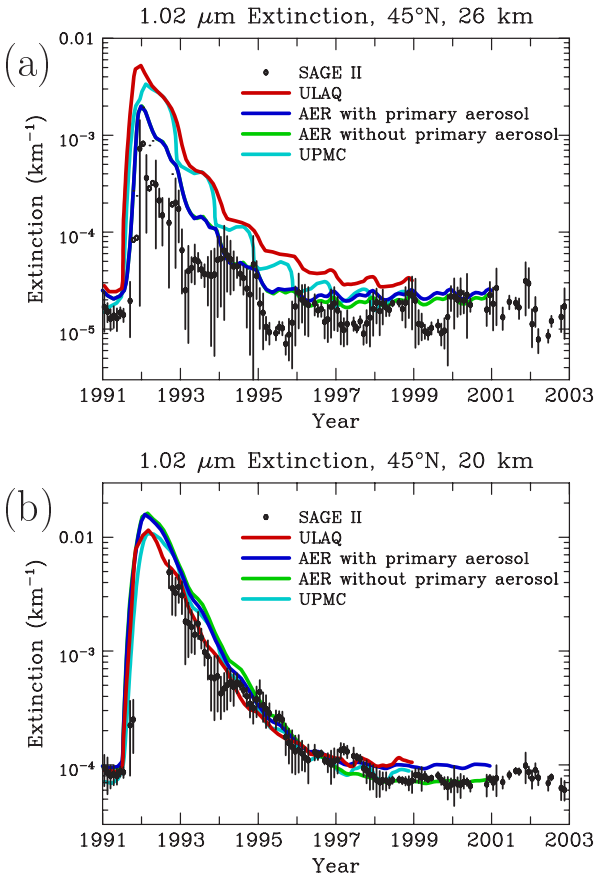

Figure 6.31: Aerosol extinction at 1.02 μm for 1991 to 2002 at (a) 45°N and 26 km and (b) 45°N and 20 km. SAGE II data are shown by symbols with error bars, model results by colored lines.

At 45°N (Figure 6.31), all the models do a good job at simulating the extinction at 20 km, but they all overestimate extinctions at 26 km compared to SAGE data. Like for the lidar data, there are significant fluctuations from one year to another in the SAGE time series. The fluctuations are visible, not only close to the background level, but also during the decay. In contrast, there is again little variability in the model-calculated extinctions, though some models obtain seasonal fluctuations at the higher altitudes which only superficially resemble observed fluctuations. Comparisons of model simulations with SAGE aerosol extinctions at 0.525 μm can be found in the supplementary material, providing a very similar overall picture.

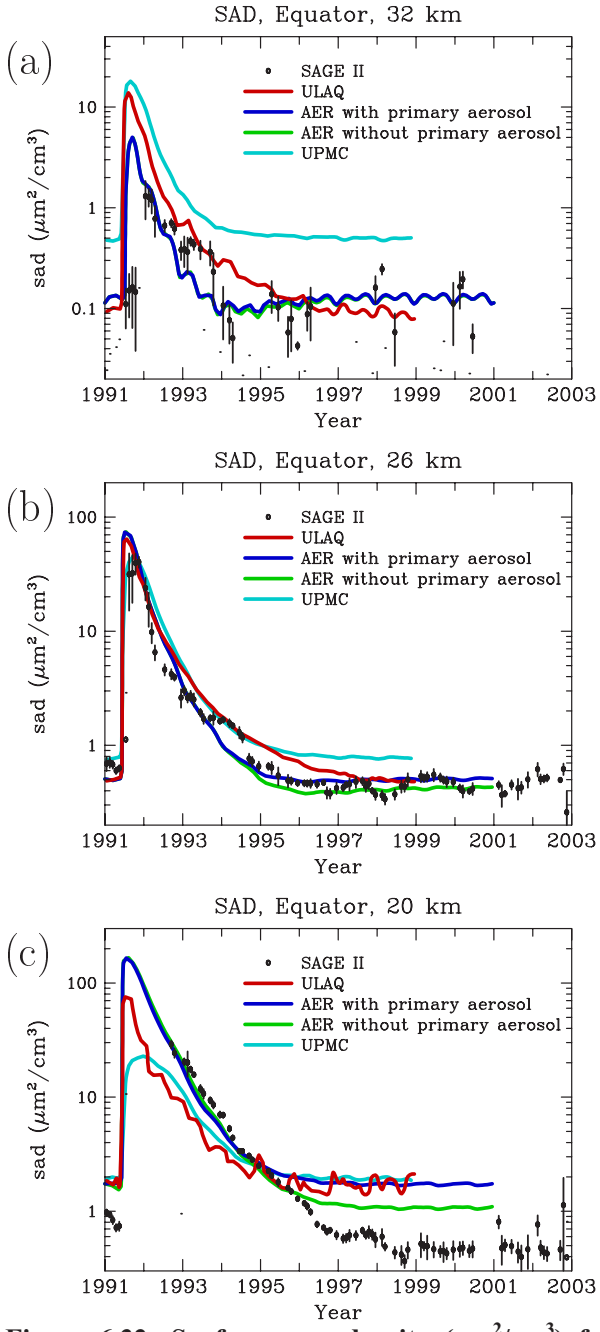

Figure 6.32: Surface area density ($\mu m^2/cm^3$) for 1991 to 2002 at the (a) equator and 32 km, (b) equator and 26 km, and (c) equator and 20 km. SAGE II results derived using Equation 4.1 are shown by symbols, model results by colored lines.

Surface area densities calculated by the models for the Pinatubo period are shown in Figure 6.32 for 20, 26, and 32 km at the equator. Model simulations follow fairly closely the surface area densities derived from SAGE II data at 26 km for the entire time period, but at 20 km they match the observations only before 1996. As seen in the surface area density comparison for background conditions, models predict surface area densities substantially higher than SAGE in the tropical lower stratosphere during periods of low aerosol loadings. This is not surprising. Small particles are abundant in this region and visible wavelength aerosol extinction is weakly sensitive to small particles. During the period of highly enhanced aerosol loading following Pinatubo, particle effective radius increases from ~0.15 to ~0.5 μm with a strongly reduced contribution from small particles to the surface area density. As a result, models and SAGE-derived surface area densities agree fairly well before 1996.

6.7.4 Comparisons with OPC Data

Model-calculated particle number concentrations are compared to measurements made with a balloon-borne optical particle counter (OPC) by Terry Deshler at the University of Wyoming [Deshler et al., 2003] between 1991 and 2003. The instrument is described in Chapter 3, Section 3.3.1, and its observations in Chapter 4, Section 4.1.3. The results are shown in Figure 6.33 at three altitudes at 41°N for particles greater than 0.15 μm. A similar comparison for particles greater than 0.25 μm can be found in the supplementary material. The UPMC and AER models do a good job of reproducing the peak number density of particles greater than 0.15 μm at 22 and 26 km, but only the UPMC model accurately captures the peak at 18 km, with the AER peak being 50% too high. The number concentration of large particles seems to return to background values by about 1995, several years earlier than for the 1.02 μm aerosol extinction.

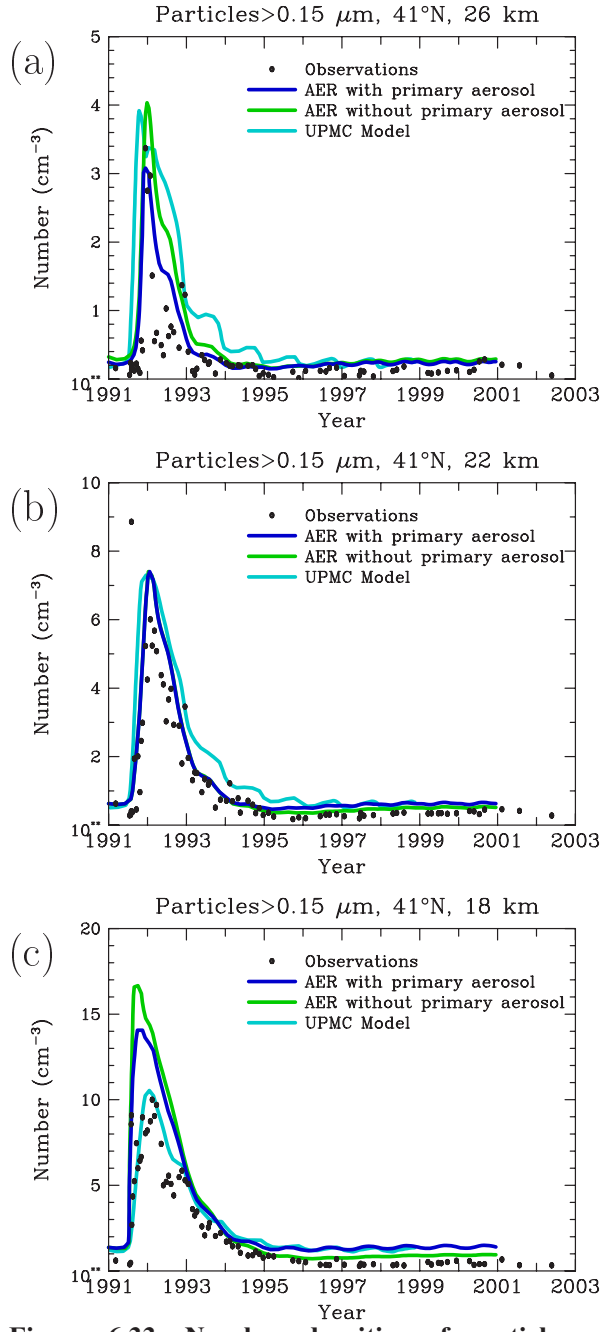

Figure 6.33: Number densities of particles with radius greater than 0.15 μm for 1991 to 2002 at (a) 26 km, (b) 22 km and (c) 18 km in Wyoming. Observations taken by balloon-borne OPC instruments [Deshler et al., 2003] at the University of Wyoming are shown by symbols, model results by colored lines.

6.7.5 Aerosol Decay Rates

E-folding Decay Timescale

This section is devoted to a detailed study of the decay of the stratospheric aerosol layer toward its background state after the volcanic eruption of Mount Pinatubo. In a sense, it is a compliment to Chapter 5 which is devoted to identifying and analyzing the background component of the stratospheric aerosol. Identifying background periods unambiguously from the observations has proven difficult, but is more straight-forward with model simulations. Models lack most sources of short-term variability, and can effectively isolate the effects of a single volcanic eruption. We focus our attention on the evolution of aerosol levels a month after the backscatter peak in order to consider the decay only. Model simulations and observations of several aerosol quantities (backscatter column, extinction, surface area density, particle number density) are shown in Figures 6.29 to 6.33. The decay of model-calculated or measured aerosol quantities toward background values tends to follow an exponential rather than linear law. For this reason, we have quantified the decay rate with an e-folding timescale, which is the time taken for an aerosol quantity to decay to 1/e of its initial value. The e-folding timescale is commonly used for quantifying the loss rate of an atmospheric constituent with respect to a specific process (e.g., chemical, dynamical, or physical process).

Apart from the long-term decay, the most obvious variations are seasonal, with an annual cycle that appears most clearly toward the end of the decay period, close to the background state (see Figures 6.29 to 6.33). There is also a substantial amount of fluctuation on inter-annual timescales in the observational time series (lidar, SAGE). As

we are only interested in the long term decay, it would be valuable to remove the scatter originating from the short-term variability in the time series. However, it is difficult to remove accurately the short-term fluctuations (such as seasonal variations) without affecting at all the long term decay in the time series because the seasonal variations are embedded into a strongly varying decay. In order to avoid any possible spurious effects from smoothing or the assumptions required for curve-fitting, we simply derive the e-folding timescale from the raw time series using the variation of the aerosol quantity monthly mean from one year to another. The e-folding decay timescale τ_{decay} is given by

$$\tau_{decay} = \frac{1}{\log[\beta(month_{(i+6)} / \beta(month_{(i-6)})]} \tag{6.1}$$

where $\beta(month_{(i)})$ is the monthly mean of an aerosol quantity in month *i*. This relationship does not provide the decay timescale over the entire time series; indeed, the timescale can only be calculated over the period of the time series truncated by 6 months at both ends. By using data points 12 months apart, Equation 6.1 removes the regular seasonal variations found in the models. Model-calculated and observational time series are processed in exactly the same way.

Decay Timescales Derived from Backscatter Column

In Figure 6.34 the e-folding decay timescale τ_{decay} is plotted as a function of time for the three lidar stations. In the figure, model results are shown by colored lines; observational data are shown with black dots. While model-calculated e-folding timescales vary relatively smoothly during the post-Pinatubo period, observational data show large variability from month to month that defies identification of a return to background on this basis. As expected, the backscatter variability is accentuated in the temporal derivative. The background variability in the lidar time series is such that the timescale, as defined by Equation 6.1, starts becoming negative from time to time in the last phase of the long-term decay. For example, negative values start appearing in 1995 at Mauna Loa. It is this short-term variance which prevents the decay timescales from tending toward high values during the last phase of the decay, after 1995-1996. This indicates that the variance from the short-term variability outweighs the variance from the long-term decay. Therefore, any timescales derived from the lidar data after about 1995 cannot provide any reliable information on the last phase of the decay and should be discarded from the analysis.

The evolution of model-calculated and lidar-based timescales show clearly that the volcanic aerosol backscatter perturbation does not decay with a constant e-folding timescale. There is, first, a short phase (about a year following the peak) during which the time scale decreases to a minimum of about 5-10 months, with general agreement between models and observations during this period. Then the decay timescale starts increasing rapidly. The evolution is very similar at the three sites in the model simulations, with the UPMC model and the AER primary aerosol model yielding almost identical e-folding times, while the AER model without primary aerosol has shorter e-folding times. Model-calculated e-folding timescales of about 1 year are reached in mid-1994 (3 years after the eruption), values of 6 years mid-1996, and a value of about 100 years mid-1998. A similar evolution is seen until 1995 in the lidar-based timescales with values reaching very approximately 1 year in mid-1994 and up to 3 years in mid-1995. After 1995, negative values of decay timescale appear. The variability in the lidar times

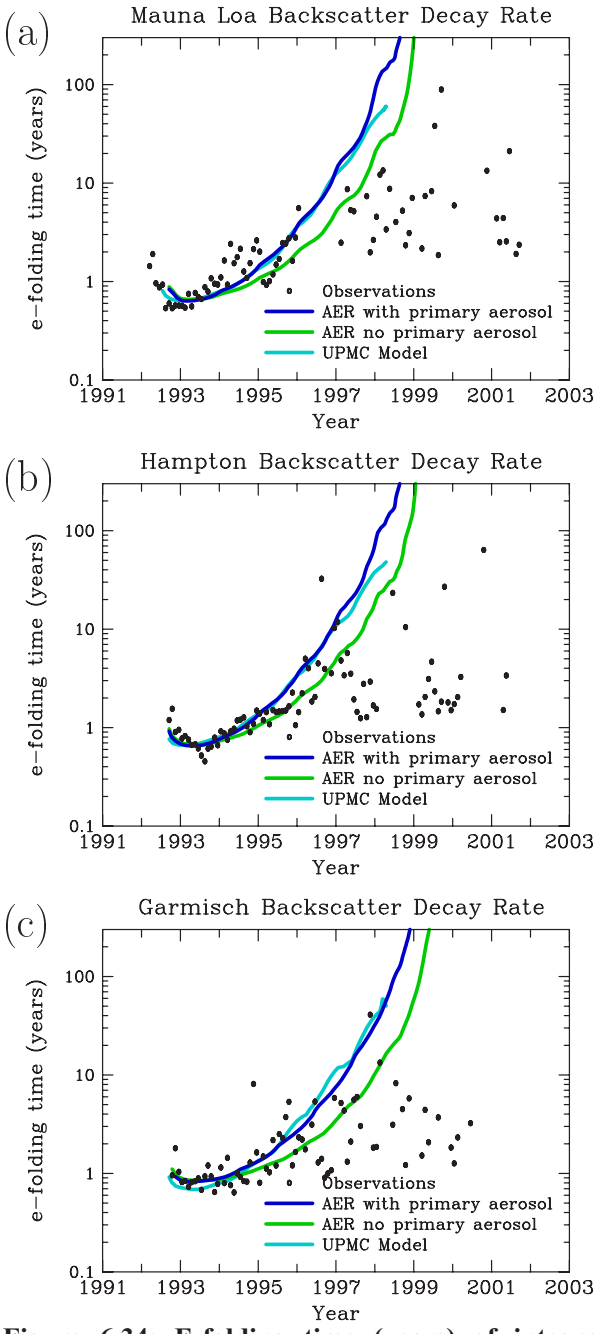

Figure 6.34: E-folding time (years) of integrated lidar backscatter at 694 nm at (a) Mauna Loa (19°N) (b) Hampton, VA, (37°N) and (c) Garmisch-Partenkirchen (47°N) for the post-Pinatubo period. Equation 6.1 applied to observations, shown by black dots, or model results, shown by colored lines, to obtain decay timescales.

series is such that no conclusions can be drawn out of the last phase of the decay. This agreement between measurements and model-simulations confirms that global models are able to simulate realistically the aerosol decay following the Mount Pinatubo eruption.

The sharp increase in the decay timescale from about 1993 originates from the drop in the mean size of the aerosol particles. Indeed, the main removal process for the aerosol particles is gravitational sedimentation. This process is highly selective with respect to the size of the aerosol particles; it is very efficient for large volcanic aerosols but has a negligible effect on the small particles. As a result, the large particles are removed very rapidly in the first phase of the decay. This is accompanied by a drop in the mean aerosol size and hence a rapidly decreasing efficiency of sedimentation during the decay.

In theory, the aerosol layer reaches the background state when the decay e-folding timescale is infinity. If the decay rate follows an exponential law, the time taken for a volcanic perturbation to vanish completely should in principle be infinity. In practice, one can choose a threshold value of the e-folding timescale beyond which aerosol changes can be neglected for the purpose of the problem considered. We choose a value of 40 years (which corresponds to a change of 2.5% per year) giving a return of model-calculated backscatters to the background level about 6.5 years after the eruption (i.e. the end of 1997 for the UPMC and AER models with primary aerosol). The AER model without primary aerosol gives slightly longer times for the return to the background level. The choice of the threshold value appears rather arbitrary. But, this does not affect much the timing of the return to the background state. Indeed, a threshold timescale value of 20 years (corresponding to a change of 5%

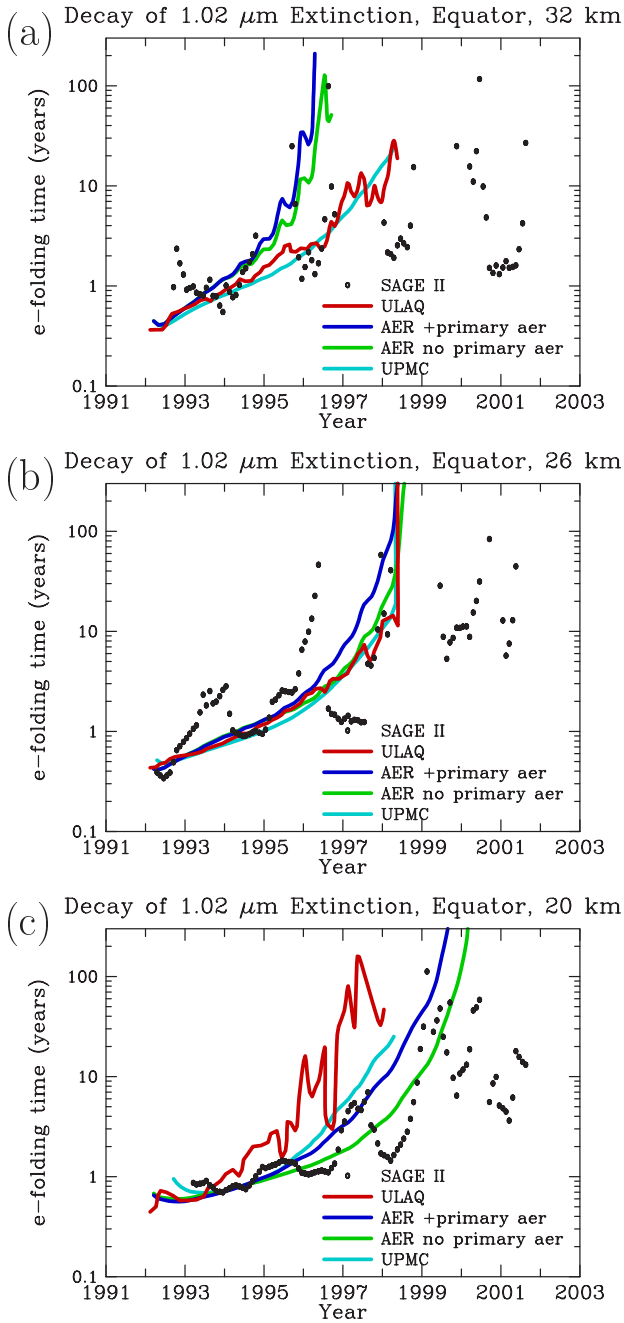

Figure 6.35: E-folding time (years) of aerosol extinction at 1.02 μm for 1991 to 2002 at the (a) equator and 32 km, (b) equator and 26 km, and (c) equator and 20 km. Equation 6.1 applied to observations, shown by black dots, or model results, shown by colored lines, to obtain decay timescales.

per year) gives a return to the background state 6 years after the eruption (i.e. mid-1997) whereas a threshold value of 80 years (corresponding to a change of 1.25% per year) gives a return to the background state 7 years after the eruption (i.e. mid-1998). It is worth pointing out that the return to the background state is sometimes established from comparisons with background levels defined a priori, for example, the aerosol levels before the volcanic eruption. The approach used here is based on the evolution of the decay timescale and does not require identifying background levels a priori.

Decay Timescales Derived from Extinction and Number Density

E-folding timescales of 1.02 μm extinction at the equator and 20, 26, and 32 km are shown in Figure 6.35. As expected, there are more differences between the model simulations for height-resolved aerosol quantities than for vertically integrated quantities such as backscatter. At the equator and 20 km, the ULAQ model predicts a more rapid increase of the timescales than the AER and UPMC models. Decay rates derived from SAGE II data tend to agree more with the AER and UPMC model simulations at this altitude. At the equator and 26 km, all models predict very similar e-folding timescales. If one assumes that the background aerosol state is reached when the extinction-based decay timescale exceeds a threshold value of 40 years (which corresponds to a change of 2.5% per year), the return to the background state occurs at the beginning of 1998 in the model simulations. At 32 km, the ULAQ and UPMC models predict a similar evolution of the e-folding timescale, while the AER model predicts a much quicker return to the background state. Assuming again a threshold value of 40 years for the timescale, the return of the 1.02 μm extinctions to background values occurs by the beginning of 1996 in the AER simulations whereas it has not occurred yet by the

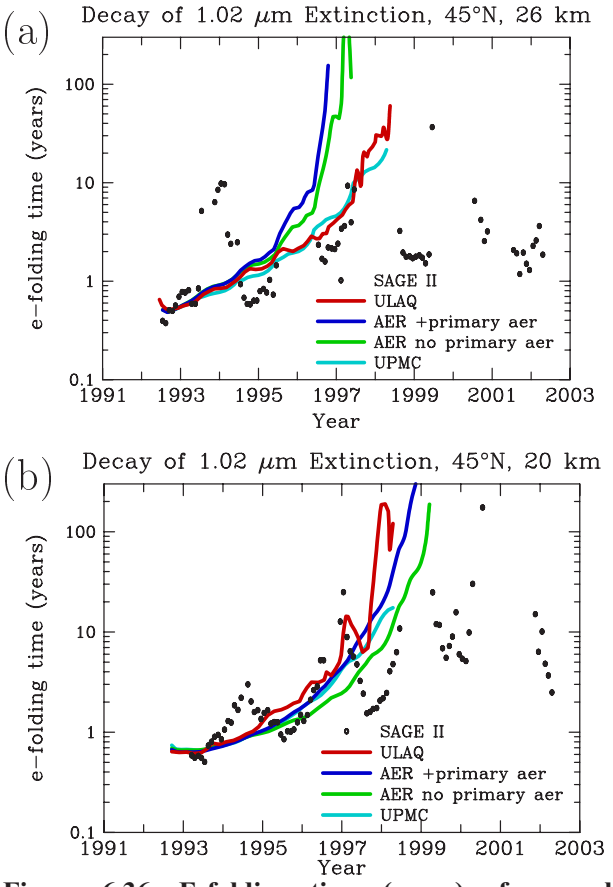

Figure 6.36: E-folding time (years) of aerosol extinction at 1.02 μm for 1991 to 2002 at (a) 45°N and 26 km and (b) 45°N and 20 km. Equation 6.1 applied to observations, shown by black dots, or model results, shown by colored lines, to obtain decay timescales.

beginning of 1998 in the ULAQ and UPMC simulations. Similar plots at 45°N are shown in Figure 6.36. The models tend to agree at 20 km but the AER model disagrees with the other two models at 26 km.

The overall evolution of the timescales derived from SAGE extinctions at the equator and at 45°N is similar to what is predicted by the models, with an increase from the minimum occurring at about 1992-1993. However, large inter-annual fluctuations are superimposed on the the overall temporal increase in the SAGE-derived timescales. For example, the timescale at 26 km and 45°N varies between 1 and 10 years in 1993-1994. The variability is such at high altitudes that no clear trend can be established after 1993-1994. At low altitudes (i.e. 20 km), the SAGE-derived timescale broadly match the evolution of the model-calculated timescale until 1997.

Figure 6.37 displays the decay rates of number density of particles greater than 0.15 μm radius at the Wyoming balloon site (41°N) at 18, 22, and 26 km. In the model simulations, background number density levels are reached as early as 1995 and by 1997 at the latest (assuming a threshold timescale value of 40 years). The fact that the large particle number density decays more rapidly than the integrated backscatter or the 1.02 μm extinction is not totally unexpected. Particles greater than 0.15 μm are strongly affected by sedimentation. Therefore, their number density should decay more rapidly than the 1.02 μm extinction which is sensitive to particles down to 0.1 μm. The 0.67 μm backscatter is sensitive to even smaller particles. There is a very strong scatter in the OPC-derived timescales at high altitudes. At 18 km, where there is much less scatter, the agreement with the AER and UPMC model simulations is satisfactory until 1995. After 1995, the large scatter precludes any meaningful comparisons.

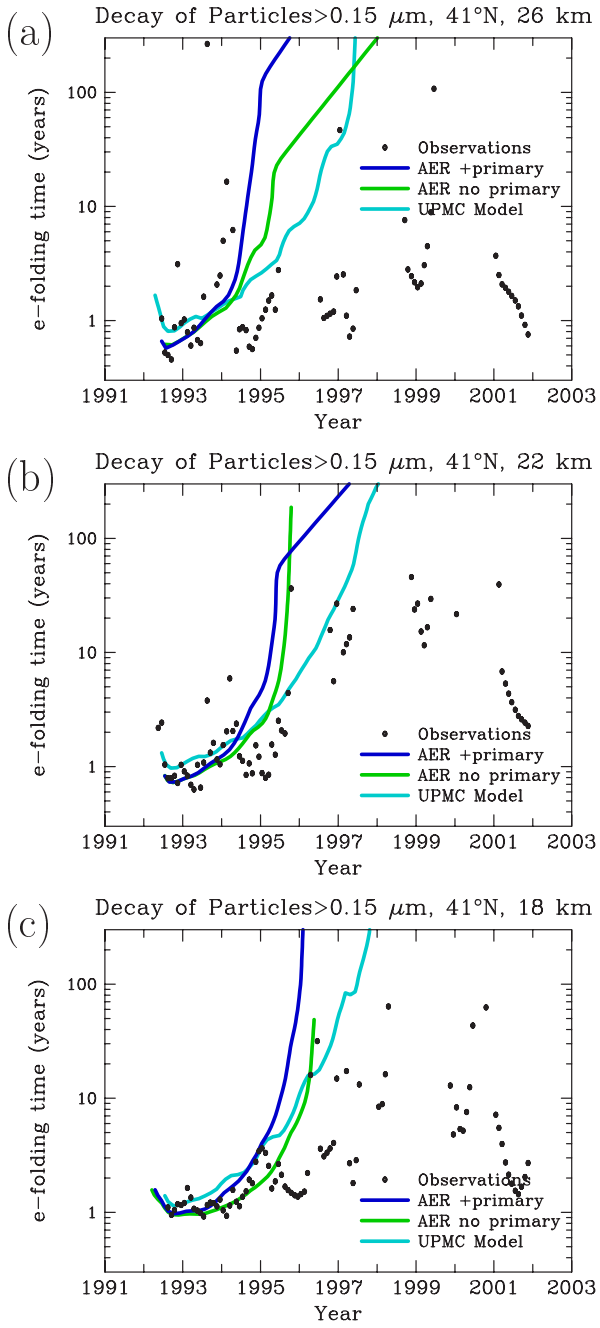

Figure 6.37: E-folding time (years) of number densities of particles with radius greater than 0.15 μm for 1991 to 2002 at (a) 26 km, (b) 22 km and (c) 18 km in Wyoming. Equation 6.1 applied to observations taken by balloon-borne OPC instruments [Deshler et al., 2003] at the University of Wyoming, shown by black dots, or model results, shown by colored lines, to obtain decay timescales.

6.8 Discussion

6.8.1 Uncertainties

Detailed comparisons of model calculations against a range of observations have been performed in this chapter. Overall, models appear to be able to reproduce most of the broad features of the distribution of stratospheric aerosols and their key precursors (OCS, SO_2). The results provide some validation of our knowledge of stratospheric sulfur sources and chemistry, and of our understanding of stratospheric aerosol processes and model parameterizations. However, the validation can only be viewed as partial for stratospheric aerosols. Indeed, the global properties of the aerosol layer are the result of complex interactions between microphysical, physicochemical and transport processes. It is very difficult to test our quantitative understanding of individual aerosol processes from comparisons against measurements of aerosol quantities that are determined by multiple processes. It is often not possible to identify unambiguously the specific cause of model discrepancies with observations or differences between model simulations.

The sensitivity studies in Section 6.6 have shown how sensitive the modeling of the background aerosol layer is to uncertainties in sulfur sources and sulfur transport to the stratosphere. Comparisons of the Mt. Pinatubo simulations with observations have shown that the models perform well under volcanic conditions. This confirms that the growth of aerosols to volcanic sizes and their subsequent removal is reproduced in a realistic way in the models. Model uncertainties are related to geographical and height resolution as well as particle size resolution. Further uncertainties stem from the implementation of gas phase and heterogeneous chemistry, microphysics, and transport. Transport is likely to be one of the largest sources of uncertainty.

In this study, we employ both 2-D and 3-D models. 2-D models are limited by their lack of an adequate tropospheric representation. The non-zonal nature of the source and sink regions of OCS and SO_2 has an impact on the transport of these gases to the stratosphere [Pitari et al., 2002; Notholt et al., 2005]. The structure of the tropical tropopause region itself is highly non-zonal in temperature, dynamics, chemistry, and cloud processing. While we have attempted to impose reasonable boundary conditions at the tropical tropopause in the 2-D models, the physics of actual stratosphere-troposphere exchange is not properly parameterized. The limited resolution of 3-D models results in inadequacies in this regard as well. Small-scale transport features such as convective cells, outflow regions, and slowly rising air parcels traveling large distances close to the local tropopause are not properly resolved in global models although they are important to the entry of tropospheric gases into the stratosphere. The effects of cloud processing on trace gases and aerosols in the upper troposphere are not well understood. Heterogeneous conversion of SO_2 to H_2SO_4 to aerosol sulfate occurs on cloud droplets and is the most important sulfate source in the troposphere. However, the small fraction of sulfate left in the atmosphere rather than removed by rain has not been observationally estimated on a global basis.

Much of our understanding of precursor gas chemistry and aerosol microphysics is based on theory and laboratory studies rather than atmospheric observations. While there is evidence that, in terms of aerosol total mass, only sulfuric acid and water (and nitric acid in cold polar regions) are important aerosol components in the stratosphere, tropospheric aerosols also contain dust, soot, organics, ammonia, and sea salt. These components are present in upper tropospheric aerosol and in trace amounts also in lower stratospheric aerosol [Murphy et al., 1998]. They influence aerosol properties and size distributions in the lower stratosphere. Interactions between sulfate aerosols and cirrus ice particles may also be important in the TTL region. Size distributions are determined by a combination of nucleation rates, coagulation rates, condensation rates, local water vapor concentrations, transport, and sedimentation. Size distributions have not been observationally verified in most of the stratosphere. Observations in the lowermost stratosphere are limited to coarse size resolution of particles greater than 5 nm in radius. One surrogate for size resolution observations is the ratios of extinctions at different wavelengths. The models do not accurately match the vertical profile of extinction ratios. Model sensitivity to bin resolution or nucleation rate does not explain this deficiency.

Transport is a major cause of uncertainty in global modeling. This is evident in comparisons between models and comparisons between models and observations. The two 3-D models use circulation parameters calculated by a GCM, with aerosol microphysics implemented within the GCM for the MPI model, the UPMC and LASP model use self-consistent 2-D transport calculated interactively, and the AER model uses a 2-D climatology of transport derived from observations. Interannual variability is not present in most of these models. Intermodel transport variability is most clearly seen in the comparison of OCS profiles in Figure 6.10. While OCS profiles at the equator vary little between models, the same profiles at 65°N show considerable variability. The transport time from the tropical tropopause to the tropical lower stratosphere is short (months) and the local lifetime of OCS long (years), and therefore little intermodel variability is evident in OCS in the tropics, whereas longer transport times and greater variability are evident at 65°N. The shorter chemical lifetime of SO_2 and the variability of OH concentrations between models result in large intermodel variability in SO_2 even in the tropics. Transport variability between model-calculated aerosol extinctions is clearly

shown in the optical depth plotted on a linear scale (Figures 6.18-6.21). No model consistently reproduced the observed latitudinal variability of optical depth for a range of altitudes. We can consider this variability between models as a proxy for the uncertainty in model transport, since each model uses an independently-derived transport circulation. The true uncertainty is unknown and probably larger than intermodel differences, given that most models predict shorter mean ages of stratospheric air than observations indicate [Waugh and Hall, 2002].

In summary, a large fraction of the uncertainties in the description of the stratospheric aerosol layer may be traced back to the modeling of transport in the lower stratosphere and in the tropopause region. While 3-D models represent this transport much more realistically than 2-D models, even they have difficulties resolving mesoscale processes close to the tropical tropopause. This might be related to the single largest uncertainty highlighted in this chapter, the large scatter of the models under volcanically quiescent conditions in the tropical upper troposphere/lower stratosphere region (e.g., Figure 6.14). This uncertainty is further complicated by the observational difficulty of safely excluding subvisible clouds from the satellite data and by the limited temporal coverage of near-background conditions in the SAGE II record. Conversely, both 2-D and 3-D models in general do a commendable job in describing the aerosol layer in the free stratosphere, at tropical as well as extra-tropical latitudes.

6.8.2 Future Trends of Stratospheric Sulfate Aerosols

Future changes in the distribution and global amount of stratospheric sulfate aerosols may be produced by increasing or decreasing emissions of precursor gases (OCS, SO_2), changes in the emission pattern of these gases, and circulation changes associated with changing climate conditions. Changes in stratospheric aerosol would, in turn, modify stratospheric ozone concentrations through heterogeneous chemistry. Changes in both ozone and aerosols would alter patterns of stratospheric heating and in turn modify stratospheric temperatures and circulation patterns.

Tropospheric SO_2 originates from both natural (volcanoes, oceans, biomass burning) and anthropogenic (fossil fuel) sources, and its distribution shows a strong geographical dependence. Anthropogenic emissions represent approximately 65-75% of the total amount [Spiro et al., 1992; Houghton et al., 2001]. Deep convective uplift is the primary mixing mechanism for tropospheric SO_2 and is particularly efficient in the tropics and over mid-latitude continental regions during summertime. For these reasons, future trends of anthropogenic sulfur released in the tropics may affect the amount of upper tropospheric SO_2 available for upward transport in the stratospheric tropical pipe and perturb the lower stratospheric budget of sulfate aerosols. According to Notholt et al. [2005] the emissions from tropical and subtropical Asia including China and India may already have started to influence the amount of sulfur-containing gases reaching the stratosphere through the "stratospheric fountain" region over the Maritime Continent and Western Pacific. OCS in the tropical upper troposphere may be enhanced by increases in biomass burning [Notholt et al., 2003].

Pitari et al. [2002] have used the ULAQ climate-chemistry coupled model to study the sensitivity of stratospheric aerosols to changing anthropogenic emissions of SO_2. They have found a global stratospheric mass density increase in 2030 with respect to 2000 of 35% and 7%, for IPCC-SRES scenarios A2 and B1 [Nakicenovic et al., 2001], respectively. In the latter case, the amount of stratospheric aerosols is found to increase,

even though the global anthropogenic sulfur flux decreases from 69 Tg-S/yr in 2000 to 53.5 Tg-S/yr in 2030. The reason lies in regional changes of sulfur emissions. Pollution regulation in mid-latitude western industrialized countries is decreasing the amount of SO_2 released, while the opposite is taking place in developing countries, mostly located at tropical latitudes (India, China, Middle East, Africa, Central and South America). The study of Pitari et al. [2002] indicates that these increasing tropical emissions of anthropogenic sulfur may be responsible for significant changes in stratospheric sulfate aerosol mass and surface area density through efficient convective uplift of surface SO_2 to the tropical tropopause, where the middle atmosphere is fed through the stratospheric tropical pipe. Surface area and mass density are predicted to increase in the Northern Hemisphere 100-200 mb layer by about 0.5 $\mu m^2/cm^3$ and 50 ng/m^3, respectively. This potential future increase of aerosol surface area density may be important for the lower stratospheric ozone photochemistry, via heterogeneous chemical reactions involving NO_x and chlorine and bromine oxides.

Besides changes in the emission patterns, changes in atmospheric circulation may also affect the future stratospheric aerosol layer. Little is known about this. Butchart and Scaife [2001] suggested that the mean meridional circulation might accelerate in a future greenhouse climate. Using a global climate model they predicted that, in response to the projected changes in greenhouse gas concentrations during the first half of the twenty-first century, the rate of mass exchange will increase by 3% per decade. This increase is due to more vigorous extratropical planetary waves emanating from the troposphere. All other things kept constant, if this acceleration actually happened, the resulting faster resupply of sulfur would make the role of particle sedimentation relatively less important, leading to higher total sulfur mixing ratio (falling in between the two lines in Figure 6.5) and consequently a larger optical depth of the stratospheric aerosol layer. Pitari et al. [2002] simulated the effect of changing climate in 2030 on the future sulfate layer. Changes in greenhouse gases produced a warmer troposphere, cooler stratosphere, and increased the residual mean vertical velocities in the tropical stratosphere. Compared with an atmosphere in which dynamics and temperature remained unchanged from 2000, the 2030 atmosphere produced a slightly smaller stratospheric burden of both SO_2 and aerosol. The expected increase in aerosol burden due to increased circulation strength may have been overwhelmed by other factors, such as changes in H_2O, OH, temperature, or convection.

Changes in aerosol may impact atmospheric temperature and circulation due to absorption or scattering of sunlight, or changes in cloud properties which could change atmospheric reflectivity. Indeed, changes in aerosol amount due to the Mt. Pinatubo eruption have been found to increase the tropical lower stratospheric temperatures [Labitzke, 1994] and to decrease the tropical ozone column [Schoeberl et al., 1993]. Changes in stratospheric circulation due to the Pinatubo eruption have been found in model experiments [Pitari and Mancini, 2002]. Long-term trends in aerosol could have similar but more modest effects.

6.8.3 Conclusions

The models are successful in reproducing observed concentrations of OCS in the tropics. Because OCS is the primary sulfur source above 25 km, and its chemical loss is primarily tropical, this provides confidence in the simulated total sulfur mass in the middle stratosphere. We have less confidence in model predictions of sulfur in the lower stratosphere. SO_2 measurements for the tropical lower stratosphere under nonvolcanic

conditions are not yet possible from satellite instruments. Such measurements of SO_2 in the tropics between 12 and 30 km over several seasons will be necessary to quantify the importance of transported tropospheric SO_2 to the stratospheric sulfur budget. Uncertainty also remains regarding the importance of primary aerosol from the troposphere.

Models reproduce observed extinction from satellite instruments with mixed success. Observed extinctions under nonvolcanic conditions in the tropics above 25 km and at midlatitudes above 20 km are within the SAGE II error bars at 0.525 and 1.02 μm for most models, but only the UPMC model comes close to reproducing the 5.26 μm extinctions measured by the HALOE instrument. Extinctions are not reproduced well in the tropical lower stratosphere. It appears that the primary aerosol distribution imposed at the tropopause may need to be refined to match extinction measurements at the SAGE II wavelengths under background conditions. The FCAS measurements used to obtain the tropopause aerosol distribution (S.-H. Lee, private communication) were an average over observations taken between 1996 and 1999 and therefore likely contain some residual effects of the Pinatubo eruption, whereas the model comparisons employ a composite of SAGE II observations over the 2000-2001 period, when volcanic influence is absent. Further observations of aerosol size and composition in the tropics up to 23 km are needed to determine the cause of the model discrepancy.

Model comparisons with lidar column observations at three sites have verified that models correctly reproduce the rise and decay of integrated aerosol backscatter and mass under volcanic conditions. Comparisons with SAGE II data during the Pinatubo period also show good agreement with models, though not consistently at all altitudes. We have shown that volcanic aerosol decays with a non-constant e-folding time which lengthens as aerosol effective radius drops. Because the models used here lack significant interannual variability in transport, model decay rates can be analyzed more easily than observations. We find e-folding rates of less than one year before mid 1994, reaching values of 40 years between 1997 and 1999. This methodology allows us to determine when volcanic aerosols have decayed to background levels with no a priori information on background levels. Observational data exhibit too much scatter to gain useful information from this method beyond 1995. A more comprehensive treatment of this issue is given in Chapter 5.

Future modeling studies should strive to include a more complete representation of upper tropospheric aerosols and relevant gas phase and heterogeneous chemistry in this region. The lower stratospheric aerosol layer is shown in our sensitivity studies to depend on input from the tropical upper troposphere. Aerosols in the upper troposphere are not purely of H_2SO_4-H_2O composition but include organics (often more than 50% by mass), mineral dust, soot, and other compounds. Organic matter in aerosols is largely absent 1-2 km above the tropopause [Murphy et al., 1998]. Vertical profiles of extinction observed by SAGE II fall sharply from high upper tropospheric values to much lower stratospheric values in only a few kilometers. This sharp gradient cannot be reproduced by any of the present models, but may be explained by a volatile component such as organics in upper tropospheric aerosols. An adequate 3-D representation of transport processes and cloud processing will be required to match aerosol observations in the troposphere-stratosphere transition region. Meteoritic material may be important to the morphology of stratospheric aerosols in polar air descending from the mesosphere, and thus should be included in future modeling studies. Reproducing the seasonal variability of aerosols remains a challenge for current models. New observations of SO_2 in the upper

troposphere and lower stratosphere, H_2SO_4 and SO_2 in the middle and upper stratosphere, and aerosol size distributions throughout the stratosphere will help to refine our understanding of stratospheric aerosols.